Biochimica et Biophysica Acta 1814 (2011) 265–276

Contents lists available at ScienceDirect

Biochimica et Biophysica Acta

journal homepage: www.elsevier.com/locate/bbapap

Proteomic identification of differentially expressed genes in neural stem cells and neurons differentiated from embryonic stem cells of cynomolgus monkey (*Macaca fascicularis*) in vitro

Kuniko Akama [a,b,*], Tomoe Horikoshi [a], Takashi Nakayama [c], Masahiro Otsu [d,e], Noriaki Imaizumi [a], Megumi Nakamura [f], Tosifusa Toda [f], Michiko Inuma [g], Hisashi Hirano [h,g], Yasushi Kondo [i], Yutaka Suzuki [i], Nobuo Inoue [d]

[a] *Department of Chemistry, Graduate School of Science, Chiba University, Chiba, Japan*
[b] *Center for General Education, Chiba University, Chiba, Japan*
[c] *Department of Biochemistry, Yokohama City University School of Medicine, Yokohama, Japan*
[d] *Laboratory of Regenerative Neurosciences, Graduate School of Human Health Science, Tokyo Metropolitan University, Tokyo, Japan*
[e] *Department of Chemistry, Kyorin University, School of Medicine, Tokyo, Japan*
[f] *Proteome, Mechanism of Aging, Tokyo Metropolitan Institute of Gerontology, Tokyo, Japan*
[g] *Advanced Medical Research Center, Yokohama City University, Yokohama, Japan*
[h] *Department of Supramolecular Biology, Graduate School of Nanobioscience, Yokohama City University, Yokohama, Japan*
[i] *Regenerative Medicine, Advanced Medical Research Laboratory, Mitsubishi Tanabe Pharma Co, Osaka, Japan*

ARTICLE INFO

Article history:
Received 28 July 2010
Received in revised form 20 October 2010
Accepted 26 October 2010
Available online xxxx

Keywords:
Embryonic stem cells
Differential expression
Neural stem cells
Neuronal differentiation
Monkey

ABSTRACT

Understanding neurogenesis is valuable for the treatment of nervous system disorders. However, there is currently limited information about the molecular events associated with the transition from primate ES cells to neural cells. We therefore sought to identify the proteins involved in neurogenesis, from *Macaca fascicularis* ES cells (CMK6 cell line) to neural stem (NS) cells to neurons using two-dimensional gel electrophoresis (2-DE), peptide mass fingerprinting (PMF), and liquid chromatography-tandem mass spectrometry (LC-MS-MS). During the differentiation of highly homogeneous ES cells to NS cells, we identified 17 proteins with increased expression, including fatty acid binding protein 7 (FABP7), collapsin response mediator protein 2 (CRMP2), and cellular retinoic acid binding protein 1 (CRABP1), and seven proteins with decreased expression. In the differentiation of NS cells to neurons, we identified three proteins with increased expression, including CRMP2, and 10 proteins with decreased expression. Of these proteins, FABP7 is a marker of NS cells, CRMP2 is involved in axon guidance, and CRABP1 is thought to regulate retinoic acid access to its nuclear receptors. Western blot analysis confirmed the upregulation of FABP7 and CRABP1 in NS cells, and the upregulation of CRMP2 in NS cells and neurons. RT-PCR results showed that CRMP2 and FABP7 mRNAs were also upregulated in NS cells, while CRABP1 mRNA was unchanged. These results provide insight into the molecular basis of monkey neural differentiation.

1. Introduction

Neural stem (NS) cells have two essential characteristics, self-renewal and multipotency to differentiate into neural cells. Transplantation of neural precursors has become one of key strategies for cell replacement in the brain. A wide range of experimental approaches have been studied, but continuous expression of oncogenes or stimulation of mitogens to proliferate NS cells, in addition to the limited plasticity and slow propagation of adult stem cells, raises question about the long-term safety of the strategy [1,2]. It has been reported that the potential to maintain dying motor neurons by delivering glial cell line-derived neurotrophic factor using human adult neural progenitor cells represents a novel treatment strategy for amyotrophic lateral sclerosis [3]. In the secretome of mouse adult

Abbreviations: ES, embryonic stem; NS, neural stem; 2-DE, two-dimensional gel electrophoresis; PMF, peptide mass fingerprinting; LC-MS-MS, liquid chromatography-tandem mass spectrometry; NSS, neural stem sphere; ACM, astrocyte-conditioned medium; FGF, fibroblast growth factor; EGF, epidermal growth factor; MAP, microtubule-associated protein; GFAP, glial fibrillary acidic protein; IPG, immobilized pH gradient; IEF, isoelectric focusing; T-TBS, TBS containing 0.05% Tween; MS, mass spectrometry; ACN, acetonitrile; TFA, trifluoroacetic acid; FABP7, fatty acid binding protein 7; CRMP2, collapsin response mediator protein 2; CRABP1, cellular retinoic acid binding protein 1

* Corresponding author. Center for General Education and Department of Chemistry, Graduate School of Science, Chiba University, Yayoi-Cho 1-33, Inage-Ku, Chiba, Chiba 263-8522, Japan. Tel.: +81 043 290 2795; fax: +81 043 290 2874.
E-mail address: akama@faculty.chiba-u.jp (K. Akama).

1570-9639/$ – see front matter © 2010 Elsevier B.V. All rights reserved.
doi:10.1016/j.bbapap.2010.10.009

bone marrow stroma-derived neural progenitor cells, Prosaposin (sulphated glycoprotein 1) has been reported to protect neural cells from toxin-induced apoptotic death [4].

On the other hand, a proteomic database for NS cells isolated from the adult rat hippocampus has been developed; using a 2-DE proteomic profiling approach, about 1100 protein spots have been mapped, of which 266 have been identified [5]. In addition, a database for the expression profiling of differentiation has been developed to identify potential cellular targets mediating the differentiation of neural stem cells [6]. Furthermore, a proteome reference map of mouse NS cells and dopaminergic neurons differentiated from ES cells has been used to identify proteins with altered expression, including translationally controlled tumor protein and α-tubulin [7]. We have assessed differentially expressed genes in mouse NS cells and neurons derived from ES cells *via* the formation of neural stem spheres (NSSs), the results of which have suggested the importance of galectin 1 in regulating differentiation [8].

Less is known, however, regarding the molecular events occurring during primate neural differentiation. Differentially expressed proteins of neurons derived from human ES cells after retinoic acid induction have been identified, including α-tubulin and vimentin [9]. Moreover, 2-DE proteome analysis of a proliferating human fetal midbrain stem cell line immortalized with the *v-myc* oncogene has been used to map 402 protein spots representing 318 unique proteins, and 2-DE proteome analysis has mapped 49 protein spots representing 45 distinct proteins during differentiation into neural cells [10]. Recently, human ES cell-derived neuroectodermal spheres were found to be enriched in cytoskeleton-associated proteins [11]. Despite these findings, however, the mechanisms of differentiation from ES cells to NS cells and neurons have not been elucidated fully.

NS cells have been produced efficiently, and at high purity, from monkey ES cells (CMK6 cell line) and from mouse ES cells *via* the formation of neural stem spheres (NSSs) under free-floating conditions in astrocyte-conditioned medium (ACM), which is readily available, easy to obtain, and ready to use [12–14]. During subsequent culture of the NSSs on an adhesive substrate with FGF-2, these Nestin-positive NS cells can be induced to migrate onto the substrate, resulting in the efficient production of large numbers of NS cells. RT-PCR analysis has shown that these NS cells express NS cell marker genes such as *Pax6*, but that expression of GFAP is undetectable. Immunofluorescence analysis has shown that almost all ($99.5 \pm 0.5\%$) of the NS cells express Nestin [15]. Furthermore, almost all of these NS cells can be differentiated into functional high-molecular-mass neurofilament protein (NF-H)-positive neurons by changing the medium from Neurobasal B-27 with FGF-2 to ACM. These neurons are found to express mRNAs encoding neuron marker genes, such as *NF-H* and *MAP2*, with expression of GFAP being less than 2.6%. Immunofluorescence has shown that almost all ($99.5 \pm 0.5\%$) of these neurons expresses NF-H and tubulin-beta III, but do not express GFAP or O4 [15]. Under these culturing conditions, astrocyte-derived factors have instructed monkey ES cells to differentiate into NS cells and neurons quickly and efficiently, although we do not know what components in ACM induce the differentiation of the ES cells into neural cells [12–15], making it difficult to identify the stimulus for neurogenesis. Multitracer assessment using positron emission tomography (PET) has shown that transplantation of NS cells induced from monkey ES cells restores dopamine function in a primate model of Parkinson's disease [15].

We have used a 2-DE-based proteomic approach to identify differentially regulated proteins in monkey NS cells and neurons derived from ES cells. We found that proteins associated with signal transduction, the cytoskeleton, stress responses, and lipid metabolism were differentially expressed during the transition from ES cells to NS cells and neurons. Together with our previous report [8], these results suggest that monkey neural differentiation is regulated in a manner similar to, but somewhat different from that of, mouse neural differentiation, and that higher neural differentiation in monkeys is regulated by more proteins than in mice.

2. Materials and methods

2.1. Cell culture

The CMK6 ES cell line of cynomolgus monkey (*Macaca fascicularis*) [16] was maintained on a feeder layer of mitotically inactivated mouse embryonic fibroblasts in DMEM medium (Invitrogen) supplemented with 1 mM 2-mercaptoethanol (Invitrogen), and 15% knockout serum replacement (Invitrogen). Colonies of undifferentiated ES cells were picked up and cultured under free-floating conditions in ACM supplemented with 20 ng/ml of recombinant human fibroblast growth factor (FGF)-2 (R&D Systems, Minneapolis, MN) and 20 ng/ml of recombinant epidermal growth factor (EGF) (R&D Systems), giving rise to NSSs as described [12–15]. The NSSs were plated onto Matrigel-coated dishes and encouraged to proliferate by culturing in Neurobasal medium (Gibco Invitrogen Corp. Grand Island, NY) supplemented with 2% B-27 (Gibco Invitrogen Corp.), 20 ng/ml FGF-2, and 20 ng/ml of EGF. Following migration of the NS cells from the adhered NSS to the surrounding areas, the NSSs were removed by picking with glass capillaries, and the migrated NS cells were harvested by treatment with trypsin. The differentiation of ES cells to NS cells was dependent on ACM, and these cells did not differentiate spontaneously. Proliferation of the Nestin-positive NS cells was dependent on FGF-2 and EGF. These cells were collected by centrifugation and suspended in Neurobasal medium. To induce neuronal differentiation, the NS cells were cultured in ACM for 8 days. Proliferation of the MAP 2-positive neurons was dependent on ACM; these cells did not differentiate spontaneously.

2.2. Immunofluorescence analysis

The cells were fixed in 4% paraformaldehyde in phosphate-buffered saline (PBS). Immunocytochemistry was performed using standard protocols [12,13] and antibodies against Nestin (Rat-4-1, Developmental Studies Hybridoma Bank) and NF-H (Sigma Chemicals, St. Louis, MO). Alexa Fluor 488- and Alexa Fluor 594-labeled secondary antibodies were from Molecular Probes (Eugene, OR). Monkey NS cells and the differentiated NS cells cultured in ACM for 1–8 days were examined using a fluorescence microscope (Eclips E800, Nikon, Tokyo, Japan) equipped with phase-contrast optics.

2.3. Sample preparation for 2-D electrophoresis

Colonies of ES cells were collected by picking with glass capillaries, whereas NS cells and neurons were collected using a cell scraper. The cells were washed twice by suspending in cold PBS followed by centrifugation at $700 \times g$ for 5 min, and stored as cell pellets at −80 °C. Aliquots of the cell pellets were suspended in lysis buffer containing 5 M urea, 2 M thiourea, 2% (w/v) 3-[3-cholamidopropyl]dimethylammonio]-1-propanesulfonate (Dojindo Laboratories, Kumamoto, Japan), 2% (w/v) sulfobetaine 10 (Amresco, Solon, OH), 2% Pharmalyte 3-10 (Amersham Biosciences Inc., Piscataway, NJ) without DTT, protease inhibitors (Pierce Chemicals, Rockford, IL) and phosphatase inhibitor cocktails 1 and 2 (Sigma-Aldrich, St. Louis, MO). The cell suspensions were sonicated five times on ice with 1-s bursts every 15 s at 25-W output, using an ultrasonic vibrator (UR200P; Tomy, Tokyo, Japan). The sonicated cells were centrifuged at $12{,}000 \times g$ for 10 min, and the supernatants were ultracentrifuged at $100{,}000 \times g$ for 30 min to remove DNA. The extracted proteins were reduced and carbamidomethylated with a ReadyPrep Reduction-alkylation kit (Bio-Rad, Richmond, CA) and desalted with a 2-D Clean-Up Kit (GE Healthcare Biosciences, Fairfield, CT) in accordance with the manufacturers' instructions. The protein content of each supernatant was measured with a 2-D Quant Kit (GE Healthcare Biosciences).

2.4. High-resolution 2-D gel electrophoresis

Proteins in the cell extract were separated according to TMIG Standard Methods in Proteomics (http://proteome.tmig.or.jp/2D/2DE_method.html) [17]. Briefly, immobilized pH gradient-isoelectric focusing (IPG-IEF) in the first dimension was performed on a reswollen Immobiline DryStrip, pH 4–7, 18 cm in length (Bio-Rad), in a CoolPhoreStar Model 3610 Horizontal IEF apparatus (Anatech, Tokyo, Japan). Aliquots of 40 μg of protein lysate per gel were loaded near the cathode wick on the IPG gel. After electrofocusing at 46,700 Vh, the IPG gel was equilibrated with SDS treatment solution (6 M urea/32 mM DTT/2% SDS/0.0025% w/v bromophenol blue (BPB)/25% v/v glycerol/25 mM Tris–HCl, pH 6.8) for 30 min. Each equilibrated gel strip was placed on top of a gel slab (7.5% T, 3% C, 20×18 cm). [%*T* means polyacrylamide gel concentration defined as percentage total monomers (i.e., acrylamide plus bisacrylamide, g/100 ml). %*C* means percentage bisacrylamide cross linker.] SDS-PAGE was run vertically in a Tris–Tricine buffer system using the CoolPhoreStar model 3068 electrophoresis apparatus (Anatech). The markers for molecular mass and p*I* were obtained from Bio-Rad and Daiichi-Kagaku (Tokyo, Japan), respectively. Proteins on gels were fixed with 40% methanol/10% acetic acid and subsequently visualized by staining with SYPRO Ruby (Molecular Probes, Eugene, OR).

2.5. Evaluation of protein patterns

2-DE gel images were scanned at an excitation wavelength of 488 nm, and emission wavelengths over 550 nm were collected on a Molecular Imager FX (Bio-Rad). Noise reduction, background subtraction, normalization, and quantitative profiling of proteins in 2-DE gels were carried out using PDQuest software version 8.0 (Bio-Rad). For spot quantification, spot volumes were calculated with the built-in feature involving the application of a fixed multiple of Gaussian radius of the spot as a background intensity function. Subsequently, relative spot intensities, defined as percentage of spot volume to the sum of total spot volumes on the parent gel, were obtained from a spreadsheet generated by the software and used for statistical analysis. All of the spots were roughly matched by an automatic program in PDQuest software, followed by a more detailed manual matching process to correct for inappropriate matching pairs, which were derived from the difference in condition of spot detection and/or the distortion of gels. Triplicate experiments were performed using three separate samples. Student's *t*-test was used to determine the significance of stage-to-stage differences. As Student's *t*-test provides valid results only when the variances of each sample are equal, a preliminary Fisher equality of variance test was applied. When variances were not equal between the two sets of data, a version of the Student's *t*-test comparison of two means including the Welch correction was used. Novel spots that appeared at a later stage were included in the comparison as increasing spots.

2.6. Mass spectrometry

In-gel digestion was performed according to the TMIG Standard Methods in Proteomics (http://proteome.tmig.or.jp/2D/2DE_method.html) [17]. Briefly, each SYPRO Ruby-stained protein spot was cut out of the gel with a spot cutter (Bio-Rad) and washed twice with 50% methanol/50 mM ammonium bicarbonate, three times with 50% acetonitrile/50 mM ammonium bicarbonate, and once with 100% acetonitrile. The supernatants were removed, and the gel fragments were dried at room temperature for 20 min. Each gel fragment was incubated in a solution of 5 μg/ml trypsin (V511A; Promega, Madison, WI) in 30% acetonitrile/50 mM ammonium bicarbonate at 30 °C overnight. The supernatants were subjected to mass spectrometry (MS). Samples (1 μl) were mixed with 1 μl of matrix solution containing 10 mg/ml CHCA (Sigma-Aldrich) in 50% acetonitrile (ACN)/40% methanol/0.1% trifluoroacetic acid (TFA), and 2-μl samples were applied to the target plate. MS analysis was performed on a MALDI-TOF mass spectrometer (AXIMA-CFR; Shimadzu, Kyoto, Japan) in reflectron mode and at a measurement range of 500–3500 *m/z*. Background noise was removed by subtraction of mass signals obtained from a control gel. Protein spots were identified by matching all the peptide masses against the Swiss-Prot and NCBInr mammal databases using Mascot Search (http://www.matrixscience.com/search_form_select.html) and MS Fit (http://prospector.ucsf.edu/ucsfhtml4.0/msfit.htm). In general, a mass tolerance of ±0.2 Da, one missed trypsin cleavage, oxidation of Met, and fixed modification of carbamidomethyl cysteine were selected as matching parameters in the search program.

For LC-MS-MS analysis, tryptic peptides were extracted with 0.1% TFA/2% ACN, with 0.1% TFA/33% ACN, and 0.1% TFA/70% ACN each once, respectively. The peptide extracts were dried on a speed-vacuum at room temperature. The peptides were dissolved in 2% ACN/0.1% formic acid, applied continuously to DiNa direct nano HPLC system (KYA Technologies, Tokyo, Japan) using autosampler DiNa AI (KYA Technologies), and separated with a gradient of buffer A (2% ACN containing 0.1% formic acid) and buffer B (80% ACN containing 0.1% formic acid), using a two-step linear gradient elution: 0–10 min, 100% of buffer A; 10–55 min, a linear gradient to 45% of B; 55–60 min, a linear gradient to 100% of B. The eluted peptides were injected directly into Q-TOF MS (Q-TOF Synapt; MA, Waters) through a nano-LC probe (ESI). Before each analysis, the instrument was calibrated with Glu 1-fibrinopeptide B. Erythromycin and Glu 1-fibrinopeptide B were used as references for molecular mass correction during each analysis. The collision gas used was argon. ProteinLynx Global Server version 2.3 (Waters) was used to create and search files with MASCOT search engine (version 2.2.04; Matrix Science) for peptide and protein identification. The search conditions were defined as tryptic peptides, and one missing cleavage was allowed. Carbamidomethylation at cysteine residues was selected as fixed modifications, and oxidation at methionine residues was selected as variable modifications. Precursor error tolerance and MS/MS fragment error tolerance were set to 30 ppm and 0.15 Da, respectively. Samples having total ion scores of less than 45 were rejected. The protein's name and accession number were reported based on SwissProt 56.0.

2.7. Western blotting

Following SYPRO Ruby staining, each 2-DE gel was washed three times with Milli-Q water for 30 min each. Each gel was incubated in 25 mM Tris/93 mM glycine/0.2% SDS for 15 min to resolubilize proteins, and the proteins were transferred onto PVDF membranes (Millipore, Bedford, MA) using a semi-dry electroblotting apparatus at ca. 2 mA/cm^2 for 1 h at room temperature in a buffer containing 25 mM Tris, 192 mM glycine, 0.08% SDS, and 20% methanol. The blotted membranes were rinsed twice with 10 mM Tris–HCl/150 mM NaCl/1 mM $CaCl_2$/1 mM $MgCl_2$, pH 7.4 (TBS), and blocked with 3% ECL blocking agent (GE Healthcare Biosciences)/T-TBS for 1 h. The membranes were rinsed twice with 0.05% Tween-20/TBS (T-TBS) and incubated with primary antibody overnight at 4 °C. The following primary antibodies were used: anti-FABP7 (rabbit anti-FABP7 polyclonal antibody, ab9558, 1:5000; Millipore), anti-prohibitin (goat anti-prohibitin polyclonal antibody, sc-18196, 1:5000, Santa Cruz Biotechnology, Santa Cruz, CA), anti-tubulin-β III (anti-neuron-specific class III β-tubulin mouse monoclonal antibody, TuJ-1, 1:10,000; TECHNE Corp.), anti-CRMP2 (rabbit anti-dihydropyrimidinase-related protein 2 polyclonal antibody, ab62661, 1:50,000, Abcam), anti-pCRMP2-T514 (rabbit anti-CRMP2 phosphorylated on Thr^{514} polyclonal antibody, ab85934, 1:1000, Abcam), anti-pCRMP2-S522 (rabbit anti-CRMP2 phosphorylated on Ser^{522} polyclonal antibody, CP2191, 1:500, ECM Biosciences), and anti-CRABP1 (rabbit anti-cellular retinoic acid binding protein 1 polyclonal antibody, ab62661, 1:5000, Abcam).

After washing three times with T-TBS, the membranes were incubated with appropriate horseradish peroxidase-conjugated secondary antibodies (goat anti-rabbit IgG, A 6154, diluted 1:5000 with 3% ECL blocking agent/T-TBS, Sigma; bovine anti-goat IgG, sc-2350, 1:5000, Santa Cruz Biotechnology; or goat anti-mouse IgG, A 4416, 1:5000, Sigma), followed by assay using an ECL Western blotting Detection System (GE Healthcare Biosciences).

2.8. Real-time RT-PCR analysis

Poly(A)$^+$ mRNA from undifferentiated ES colonies, NS cells, and neurons was prepared using QuickPrep Micro mRNA Purification Kits (GE Healthcare Biosciences). Each mRNA was reverse transcribed into cDNA using random hexamer primers, in accordance with the manufacturer's instructions (Applied Biosystems, Foster City, CA). Quantitative real-time RT-PCR was performed on an ABI PRISM 7300 (Applied Biosystems) using SYBR Green PCR Master Mix and the primer pairs shown in Supplementary Table 1, which had been designed using Primer Express software (Applied Biosystems), in accordance with the manufacturer's instructions. Expression of each target gene was normalized relative to that of GAPDH mRNA, with relative quantitative evaluation of the initial template copy number determined relative to a standard curve of GAPDH cDNA (Applied Biosystems). All samples were analyzed in five replicates.

3. Results

3.1. Differential expression of proteins during neural differentiation

To identify proteins that may be differentially regulated in monkey ES cells, NS cells, and neurons, we used highly homogeneous monkey NS cells expressing Nestin (99.5% ± 0.5%) and neurons expressing NF-H (99.5% ± 0.5%) differentiated from ES cells (CMK6 clone) by the NSS method [15]. Fig. 1 indicates the phase-contrast micrograph of monkey NS cells (Fig. 1A), the differentiating NS cells cultured in ACM for 1–8 days (Fig. 1B–F), and immunofluorescence analysis of the NS cells and neurons (Fig. 1G–J). The cells cultured in ACM for 8 days were differentiated to neurons. The NS cells and neurons used were confirmed to be highly homogeneous cells expressing Nestin (Fig. 1G and H) and NF-H (Fig. 1I and J), respectively, as well as the earlier report [15]. RT-PCR showed that these monkey ES cells expressed undifferentiated ES cell marker genes, such as *Oct4*, *Nanog*, and *Cripto*. Immunostaining indicated that these ES cells expressed Oct4, SSEA-1, Nanog, and alkaline phosphatase (data not shown). The monkey ES cells did not differentiate spontaneously on a feeder layer, and the levels of expression of Pax6, MAP2, and GFAP in ES cells by RT-PCR were 0.0%, 0.3%, and 0 %, respectively. RT-PCR showed that the relative levels of expression of Pax6, MAP2 and GFAP in NS cells were 100%, 4.6%, and 0 %, respectively. The relative levels of expression of MAP2, GFAP, and O4 in neurons were 100%, 2.6%, and 0 %, respectively.

Preliminary experiments using a broader pH range of pH 3–10 showed that about 2/3 of all spots of extracted proteins focused at pH 4–7 and about 1/3 at pH 7–10. However, the resolution of proteins on the gel was not fully satisfactory. We therefore used an IPG strip gel of pH 4–7 as the first step, which had a higher resolution at pH 4–7 than the strip gel of pH 3–10. Approximately 500 protein spots were detected by SYPRO Ruby staining. Using PDQuest software, quantitative comparisons were performed to assess the relative abundance of altered proteins on 2-D gel maps of the cells.

We obtained reproducible 2-DE profiles and relative spot intensities from all samples in experiments performed in triplicate. Fig. 2 shows typical gel maps of proteins from monkey ES cells, NS cells, and neurons. To assess changes in protein patterns among these three stages, we compared the patterns of ES cells and NS cells and the patterns of NS cells and neurons. Table 1 shows the relative intensities of the corresponding spots in two stages. In comparing NS cells and ES cells, we found 17 protein spots that were upregulated and seven that were downregulated. In comparing neurons with NS cells, we found three protein spots that were upregulated and 10 that were downregulated. These proteins were selected for subsequent analysis by MS. PMF and LC-MS-MS of the selected spots followed by a database search revealed the identities of these proteins (Table 1 and Fig. 2). Among the proteins upregulated when going from ES cells to NS cells were creatin kinase B type, peroxiredoxin-2, Rho GDP dissociation inhibitor 1, heterogeneous nuclear ribonucleoprotein K, vimentin, lamin B1, lamin B2, 14-3-3 protein zeta/delta, FABP7, annexin A5, reticulocalbin 1, CRMP2, and CRABP1; in contrast, heat shock cognate 71 kDa, glutathione S-transferase P, and prohibitin showed decreased expression when differentiating from ES cells to NS cells. Furthermore, in the differentiation of NS cells to neurons, reticulocalbin 1 and CRMP2 were upregulated, whereas Rho GDP dissociation inhibitor 1, annexin A5, elongation factor 1B, and heat shock protein 90B were downregulated. Table 2 summarizes the possible functions of the differentially regulated proteins during the differentiation from ES cells to neural cells. We classified the molecular functions of these proteins into eight groups: four were involved in the cytoskeleton; four, in stress responses; five, in signal transduction; and two, in lipid metabolism; the remainder were involved in protein metabolism, RNA metabolism, cell cycle, and energy metabolism.

Of the cytoskeletal proteins, lamin B1 and B2 and vimentin were upregulated in NS cells relative to ES cells. Lamin B1 and B2 are components of a fibrous layer on the inner nuclear membrane, whereas vimentin is part of the cytoskeleton, along with microtubules and actin microfilaments. Cytoskeletal networks have been reported to serve multiple roles in neurons [18]. Of the signal transduction-related proteins, Rho GDP dissociation inhibitor 1 and 14-3-3 zeta/delta were upregulated in NS cells compared with ES cells. Rho GDP dissociation inhibitor 1 has been reported to be involved in the regulation of the actin cytoskeleton [19]. It has been reported that the protein 14-3-3 zeta/delta is an adaptor protein implicated in the regulation of signaling pathways; this protein binds to and activates phosphorylated tyrosine hydroxylase, which catalyzes the rate-limiting step of dopamine synthesis [20]. Among the other proteins upregulated in NS cells and neurons compared with ES cells was reticulocalbin 1, which is thought to be involved in calcium signal modulation based on its amino acid sequence containing four EF hands (http://www.geneontology.org/).

We observed four spots of CRMP2 (Fig. 2, Table 1). Based on their electrophoretic mobility on 2-D gels [21], spots 1, 2, 3, and 4 of CRMP2 were thought to be non phosphorylated CRMP2 (CRMP2-1), CRMP2 phosphorylated at Ser^{522} (CRMP2-2), CRMP2 phosphorylated at Ser^{522} and Thr^{514} (CRMP2-3), and CRMP2 phosphorylated at Ser^{522}, Thr^{514}, and Thr^{509}/Ser^{518} (CRMP2-4), respectively. CRMP2-1 was upregulated during the differentiation of ES cells to NS cells, whereas CRMP2-2 and CRMP2-4 were upregulated from ES cells to NS cells and from NS cells to neurons. CRMP2 has been reported to be involved in axon guidance, neuronal growth cone collapse, and cell migration [22]. These findings suggest a probable link between active signal transduction and changes in the cytoskeleton during the differentiation from ES cells to NS cells and neurons. Phosphoproteomic analyses of human ES cells and during the early differentiation have suggested remodeling of the cellular matrix via active signal transduction based on changes in the proteins including cytoskeleton [23,24].

Of the heat shock/stress proteins, heat shock cognate 71-kDa protein and heat shock protein 90 beta were downregulated in neurons. Heat shock protein 90 beta, also known as tumor-specific transplantation antigen Hsp84, has been reported to inhibit tumor growth in animals injected with tumor antigen prior to tumor challenge [25]. Among the proteins involved in the redox regulation of cells, peroxiredoxin 2 was upregulated, while glutathione S-transferase was downregulated, in NS cells. Peroxiredoxin 2 has been also reported to protect neurons against peroxide [26]. Glutathione S-transferase has been reported to remove

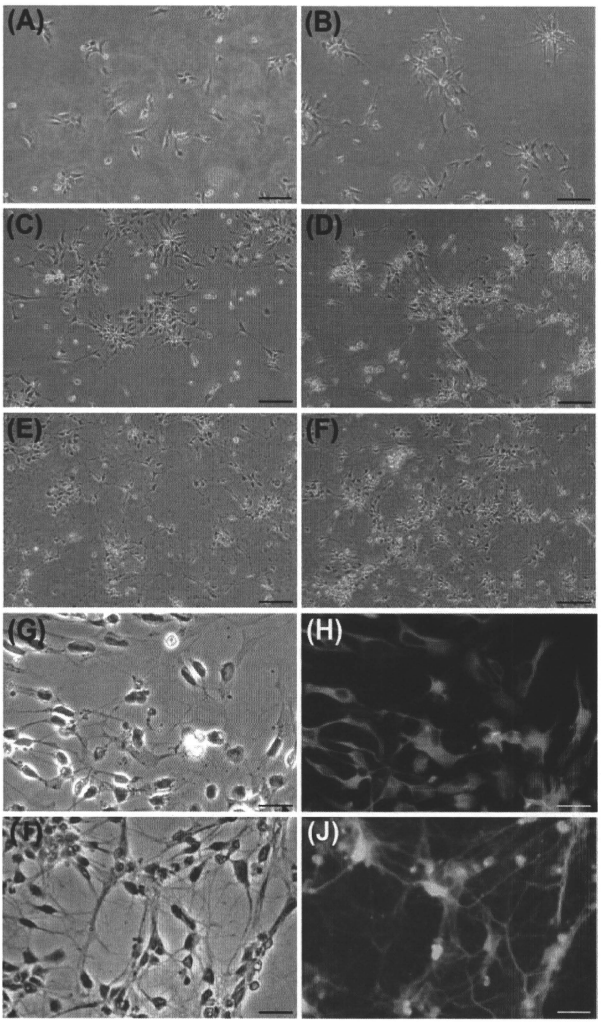

Fig. 1. Differentiation of monkey NS cells to neurons. Phase-contrast micrographs showing monkey NS cells (A), the differentiated monkey NS cells cultured in ACM for 1 day (B), 2 days (C), 4 days (D), 6 days (E), and 8 days (F). (G and I) High-magnification images of panels (A) and (F), respectively; (H and J) Nestin (orange) and NF-H (green) staining profiles by fluorescence microscope analysis of panels (G) and (I), respectively. Scale bars: (A–F) 100 μm, (G– I) 25 μm. (For interpretation of the references to color in this figure legend, the reader is referred to the web version of this article.)

wound substances by conjugation of reduced glutathione. These findings suggest that the regulation of oxidoreduction is altered in NS cells compared with ES cells.

Of the metabolism-related proteins, heterogeneous nuclear ribonucleoprotein K, which shows increased expression in NS cells compared with ES cells, has been reported to be involved in the nuclear metabolism of hnRNAs such as mRNA splicing (http://www.geneontology.org/). In contrast, both FABP7 and CRABP1 were upregulated in NS cells compared with ES cells. It has been reported that FABP7 is involved in the maintenance of NS cells and neurons [27–31], whereas CRABP1

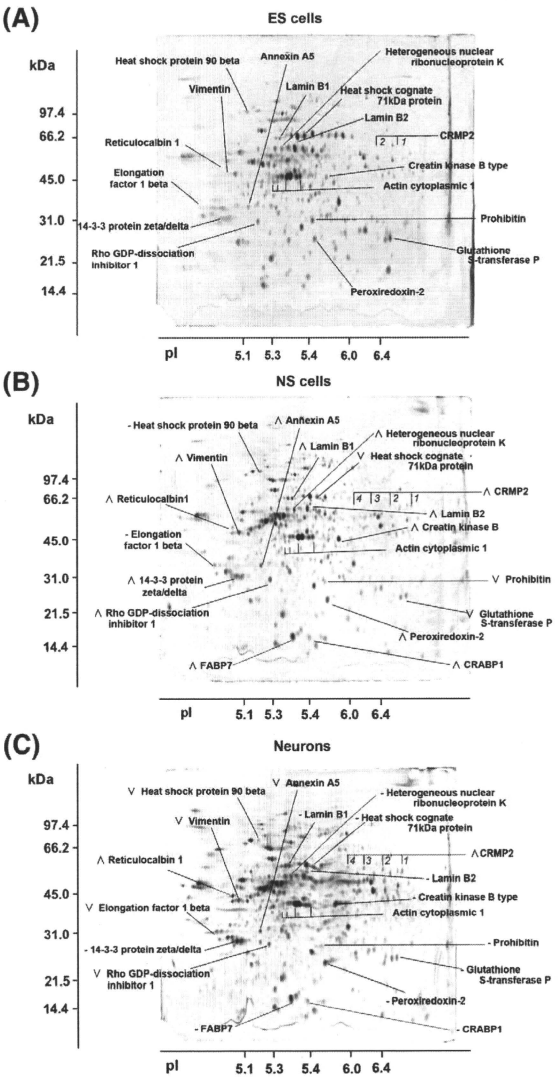

Fig. 2. 2-D protein profiles from monkey (A) ES cells, (B) NS cells, and (C) neurons. Proteins were separated based on pI (*X*-axis) and molecular mass (*Y*-axis) and visualized by staining with SYPRO Ruby. Each protein was identified by PMF and LC-MS-MS, and identified proteins with altered expression are shown on the gels. (Λ) and (V) indicate up-regulated proteins and downregulated proteins, respectively. (–) Indicates unaltered proteins.

is thought to facilitate the catabolism and/or the sequestering of retinoic acid, rendering it unavailable to nuclear receptors [32]. Retinoic acid has been reported to regulate the expression of genes involved in cell proliferation, cell differentiation, and apoptosis, and to be essential for normal embryonic development and for health in adults [33].

Table 1
Differentially expressed proteins of monkey NS cells and neurons differentiated from ES cells by the NSS method.

Ssp[a] No.	Protein name	Relative spot intensity (mean ± SD)			Quantitative changes[b]		Accession number[c]	Score[d]	Matched peptides[e]	Sequence Cov. (%)[f]
		ES cells	NS cells	Neurons	NS cells[g]	Neurons[h]				
1301	Elongation factor 1 beta	1.30 ± 0.74	1.42 ± 0.11	0.91 ± 0.19	–	−0.64 (0.05)	P24534	74/102	6/4	20/24
1309	14-3-3 Protein zeta/delta	1.78 ± 0.80	3.71 ± 0.61	4.35 ± 2.45	2.08 (0.05)	–	Q5R651	106/554	8/13	33/41
1402	Reticulocalbin 1	0.16 ± 0.14	0.98 ± 0.25	1.91 ± 0.05	6.13 (0.05)	1.95 (0.05)	Q15293	70/94	6/2	17/8
1404	Vimentin	0.31 ± 0.12	3.20 ± 0.19	2.29 ± 0.15	10.3 (0.01)	−0.72 (0.01)	Q4R4X4	213/1155	20/30	48/48
2401	Vimentin	NA[i]	3.32 ± 0.58	1.89 ± 0.24	▲ (0.05)	−0.57 (0.05)	Q4R4X4	304/861	30/25	64/48
2402	Vimentin	0.13 ± 0.18	0.89 ± 0.20	0.30 ± 0.10	6.85 (0.01)	−0.34 (0.01)	Q4R4X4	116/505	8/16	27/35
2403	Vimentin	NA[i]	2.77 ± 0.47	1.52 ± 0.05	▲ (0.01)	−0.55 (0.05)	Q4R4X4	354/1036	34/32	71/53
3508	Vimentin	0.79 ± 0.87	3.13 ± 0.90	3.53 ± 1.78	3.96 (0.05)	–	Q4R4X4	171/492	13/15	39/28
4503	Heterogeneous nuclear ribonucleoprotein K[j]	1.39 ± 0.19	1.95 ± 0.25	1.56 ± 0.72	1.40 (0.05)	–	Q4R4N6	883	25	34
2206	Rho GDP dissociation inhibitor 1	1.70 ± 0.01	2.52 ± 0.26	1.64 ± 0.17	1.47 (0.05)	−0.65 (0.01)	Q4R4J0	129/256	9/7	38/25
2303	Annexin A5	1.07 ± 0.07	1.76 ± 0.05	1.20 ± 0.20	1.64 (0.01)	−0.68 (0.05)	Q4R4H7	73/281	5/11	16/29
2702	Heat shock protein 90 beta	0.77 ± 0.18	0.74 ± 0.07	0.33 ± 0.18	–	−0.45 (0.05)	Q4R520	83/936	14/23	20/27
3306	Actin cytoplasmic 1	0.82 ± 0.03	0.53 ± 0.13	0.17 ± 0.02	–	−0.32 (0.05)	Q4L0Y2	79/155	8/6	28/21
3308	Actin cytoplasmic 1	0.87 ± 0.14	0.47 ± 0.11	NA[i]	−0.54 (0.05)	–	Q4L0Y2	68/474	5/11	16/37
4401	Actin cytoplasmic 1	4.03 ± 0.80	2.25 ± 0.28	1.22 ± 0.40	−0.56 (0.05)	−0.54 (0.05)	Q4L0Y2	105/414	8/15	24/40
5403	Actin cytoplasmic 1	4.23 ± 0.46	2.95 ± 0.32	2.48 ± 0.78	−0.70 (0.05)	–	Q4L0Y2	90/419	6/14	18/47
4201	FABP7	NA[i]	7.35 ± 1.39	7.15 ± 1.13	▲ (0.05)	–	Q15540	169/307	10/5	83/36
4602	Lamin B1	0.93 ± 0.05	1.76 ± 0.13	1.88 ± 0.04	1.83 (0.01)	–	P20700	107/1295	11/35	19/38
4611	Heat shock cognate 71-kDa protein	2.18 ± 0.22	1.50 ± 0.26	1.50 ± 0.32	−0.69 (0.05)	–	A2Q0Z1	84/813	7/25	13/31
5606	Heat shock cognate 71-kDa protein	3.28 ± 0.64	1.81 ± 0.36	2.34 ± 0.44	−0.55 (0.05)	–	A2Q0Z1	66/614	6/19	11/25
5201	Cellular retinoic acid binding protein 1	NA[i]	1.55 ± 0.37	1.15 ± 0.17	▲ (0.05)	–	P29762	119/360	6/10	48/47
5207	Prohibitin	2.05 ± 0.39	0.70 ± 0.20	0.56 ± 0.06	−0.34 (0.01)	–	Q3T165	238/283	16/8	58/36
5210	Peroxiredoxin-2	2.16 ± 0.50	3.60 ± 0.46	3.59 ± 1.37	1.67 (0.01)	–	Q5RC63	185/341	11/8	47/33
5603	Lamin B2	0.39 ± 0.11	0.71 ± 0.05	0.80 ± 0.24	1.82 (0.05)	–	Q03252	151/509	21/14	35/21
6306	Creatin kinase B type	1.14 ± 0.05	4.74 ± 0.47	4.36 ± 0.44	4.16 (0.01)	–	P12277	154/517	14/11	43/30
6614	CRMP2-4[k]	NA[i]	0.11 ± 0.04	0.36 ± 0.05	–	3.27 (0.01)	O08553	63/356	5/10	13/21
7603	CRMP2-3[l]	NA[i]	0.24 ± 0.08	0.55 ± 0.02	–	2.29 (0.05)	Q5R9Y6	108/188	9/7	21/16
8503	CRMP2-1[m]	0.16 ± 0.11	0.78 ± 0.25	1.23 ± 0.42	4.38 (0.05)	–	Q5R9Y6	121/287	12/8	25/18
8203	Glutathione S-transferase P	3.28 ± 0.23	1.55 ± 0.22	1.26 ± 0.15	−0.47 (0.01)	–	Q28514	66/306	4/7	27/38

[a] Special spot number on 2-DE gel (Fig. 2) obtained by using PDQuest software version 8.0 (Bio-Rad).
[b] The values show the fold increase of proteins toward the older developmental stage. The minus (−) values show their fold-decrease. Novel protein spots that appeared at a later stage were included in the comparison as increasing spots, and their upregulation is shown by (▲). (–): No change.
[c] Swiss-Prot accession numbers are given for proteins.
[d] Score that resulted from PMF/LC-MS-MS search (http://www.matrixscience.com/search_form_select.html) is calculated as described in the web site (http://www.matrixscience.com/help/scoring_help.html). Score in PMF is $-10*\mathrm{Log}(P)$, where P is the probability that the observed match is a random event. Protein scores greater than 61 are significant ($p<0.05$). In LC-MS-MS search, ion score is $-10*\mathrm{Log}(P)$, where P is the probability that the observed match is a random event. Individual ion scores >35 indicate identity or extensive homology ($p<0.05$). Protein scores are derived from ions sores as a non-probabilistic basis for ranking protein hits.
[e] Numbers of matched peptides that resulted from PMF/those that resulted from LC-MS-MS search obtained by using Mascot Search.
[f] Sequence coverage that resulted from PMF/that resulted from LC-MS-MS search.
[g] ES cells vs. NS cells. For protein spots that showed statistical significance, the P-values are shown in parentheses (t-test).
[h] NS cells vs.neurons. For protein spots that showed statistical significance, the P-values are shown in parentheses (t-test).
[i] NA: not detectable on the gel.
[j] Identified by LC-MS-MS search.
[k] Spot 4 of CRMP2 in Fig. 2.
[l] Spot 3 of CRMP2 in Fig.2.
[m] Spot 1 of CRMP2 in Fig.2.

3.2. Comparison of protein and mRNA expression levels

To investigate the levels of expression of the mRNAs encoding the identified proteins, we performed real-time RT-PCR analyses for reticulocalbin 1, FABP7, CRMP2, and CRABP1 [Supplementary Table 2]. Fig. 3 shows a comparison of protein and mRNA expression. The levels of expression of FABP7 and reticulocalbin 1 mRNA were altered in a manner similar to that of the respective protein expression levels (Fig. 3A, B). We found that the level of expression of CRMP2 mRNA (Fig. 3D) was upregulated from ES cells to NS cells in a similar manner to the level of expression of CRMP2-1 (non-phosphorylated CRMP2 protein). In contrast, the levels of CRMP2 mRNA were similar in NS cells and neurons, whereas the levels of expression of CRMP2-2 and CRMP2-4 proteins were increased during this differentiation step. We also found that the level of expression of mRNA encoding CRABP1 (Fig. 2C) was unchanged, differing from the changed level of expression of the encoded protein.

We found that the expression patterns of CRABP1 and CRMP2 mRNAs and proteins (Fig. 3C and D) differed. These proteins were of interest, in that they are involved in regulating neural differentiation. CRMP2 has been shown to be involved in axon guidance, neuronal growth cone collapse, and cell migration [22], whereas CRABP1 has been reported to be involved in tightly regulating the cellular concentrations of retinoic acids, which is particularly important in the development of the central nervous system [33]. We found that prohibitin was downregulated in monkey NS cells and neurons compared with ES cells (Fig. 2 and Table 1), whereas prohibitin is upregulated in mouse NS cells and neurons compared with mouse ES cells [8,34].

To confirm the differential expression of CRMP2, CRABP1, and prohibitin, we performed 2-D Western blotting analyses of these proteins, together with FABP7 and tubulin βIII as marker proteins of NS cells and neurons, respectively, using the same specimens we used for 2-DE. We found that the expression of FABP7 and CRABP1 was upregulated, whereas the expression of prohibitin was downregulated, in NS cells and neurons (Fig. 4). Western blotting analysis showed that CRMP2-1 was upregulated in NS cells, and CRMP2-2, CRMP2-3, and CRMP2-4 were upregulated in NS cells and neurons (Fig. 4E). These results were consistent with the data obtained by 2-DE except for the upregulation of CRMP2-3, which was not detected by SYPRO Ruby staining, perhaps due to overlap with other proteins.

The phospho-CRMP2 immunoblotting of neurons (Fig. 4F) indicated that CRMP2-1, CRMP2-2, and CRMP2-3 were non-phosphorylated, mono-phosphorylated on Ser^{522}, and di-phosphorylated on Thr^{514}

Table 2
Proteins with altered expression during the differentiation from monkey ES cells to NS cells and neurons by the NSS method. Molecular functions and possible roles in neurogenesis are shown for the proteins identified in this study. Molecular functions were obtained from the Gene Ontology Consortium (http://www.geneontology.org/). Listed proteins were classified into eight groups: D, cytoskeleton; C, heat shock/stress proteins; S, signal transduction; PM, protein metabolism; LM, lipid metabolism; EM, energy metabolism; RM, RNA metabolism; E, cell cycle.

Protein name	Class	Function	Neurogenesis	Ref.
Elongation factor 1 beta	PM	Catalytic subunit of the guanine nucleotide exchange factor of the eukaryotic elongation factor 1 complex	Not known	–
14-3-3 Protein zeta/delta	S	Adaptor protein implicated in the regulation of signaling pathway	Activates the tyrosine hydroxylase catalyzing rate-limiting step of dopamine synthesis	[20]
Reticulocalbin 1	S	Contains four functional EF-hand domains and regulates calcium-dependent activities in endoplasmic reticulum	Not known	–
Vimentin	D	Class-III intermediate filaments interspecies interaction between organisms	Increased in NS cells	[10]
Hetrogeneous nuclear ribonucleoprotein K	RM	Plays a role in the nuclear metabolism of hnRNAs with cytidine-rich sequences, such as mRNA splicing	Decreases during neuronal differentiation from the human NS cell line	[10]
Rho GDP dissociation inhibitor 1	S	Regulation of GDP/GTP exchange reaction of Rho to maintain Rho proteins in an inactive state	Present in human NS cell lines	[6,10]
Annexin A5	S	Calcium-dependent binding to phospholipid membranes, interacts selectively with a receptor that possesses protein tyrosine kinase activity	Not known	–
Heat shock protein 90, beta	C	Processes and transports secreted proteins	Present in human NS cells	[6,10]
Actin cytoplasmic 1	D	ATP-binding structural constituent of cytoskeleton	Increases during neuronal differentiation from the human NS cell line	[10]
Fatty acid binding protein 7	LM	Fatty acid-binding activity involved in transport or propagation of processes extending from the cell	Maintenance of neuroepithelial cells of rat cortex. Functional links to glutamate receptor	[27–31]
Lamin B1	D	Components of the nuclear lamina, a fibrous layer on the nucleoplasmic side of the inner nuclear membrane	Decreases during neuronal differentiation from the human NS cell line	[10]
Heat shock cognate 71-kDa protein	C	Molecular chaperone	Decreases during neuronal differentiation from the human NS cell line	[10]
Cellular retinoic acid binding protein 1	LM	Binds retinoic acid and regulates the access of retinoic acid to nuclear retinoic acid receptors	Increases in human ES cell-derived neuroectodermal spheres	[11]
Prohibitin	E	Inhibition of DNA synthesis to regulate proliferation	Increases during neural differentiation from mouse ES cells	[8,34]
Peroxiredoxin-2	C	Redox regulation of the cell	Increases during retinoic acid-induced neural differentiation from mouse ES cells	[9]
Lamin B2	D	Components of the nuclear lamina, a fibrous layer on the nucleoplasmic side of the inner nuclear membrane	Not known	–
Creatine kinase B type	EM	Catalysis of transfer of phosphate between ATP and various phosphogens	Increases during neuronal differentiation from the human NS cell line	[8,10]
Collapsin response mediator protein 2	S	Plays a role in axon guidance, neuronal growth cone collapse, and cell migration	Present in rat and human NS cells	[6,10]
Glutathione S-transferase P	C	Removes wound substances by conjugation of reduced glutathione	Decreases during neuronal differentiation from mouse ES cells	[7]

and Ser^{522}, respectively, and suggested that CRMP2-4 was triphosphorylated on Thr^{514}, Ser^{522} and X (undetermined acid residue). These results were consistent with the report of Patrakitkomjorn et al. [21].

Comparisons of protein and mRNA expression levels suggested that the upregulation of CRABP1 protein in NS cells and the upregulation of CRMP2-2, CRMP2-3, and CRMP2-4 in NS cells and neurons also occurred at the post-transcriptional level.

4. Discussion

In this study, we examined differentially regulated proteins in monkey NS cells and neurons derived from ES cells. Using highly homogeneous cells differentiated from ES cells via the formation of NSS, we identified 17 proteins with increased expression and seven with decreased expression from ES cells to NS cells, and three proteins with increased expression and 10 with decreased expression in going from NS cells to neurons.

Among the proteins identified, some have been reported to be differentially regulated in mammalian neurogenesis from ES cells to neural cells. For example, the expression of creatine kinase B type is increased in neural cells differentiated from the human NS cell line ReNcell VM [10]. Glutathione S-transferase P is downregulated from mouse ES cells to neurons [7]. FABP7, which is expressed in neuroepithelial cells, including NS cells and differentiating neurons downstream of the transcription factor Pax6, is essential for their maintenance during early embryonic development of the rat cortex [27]. FABP7 is expressed in mouse radial glia, which serve as neuroprogenitors in the adult mouse brain [28]. Moreover, FABP7 is strongly expressed in radial glia and immature astrocytes in pre- and perinatal brain, but its expression is remarkably attenuated in the astrocytes of adult rat brain [29]. Fabp7 has functional links to the glutamate receptor, *N*-methyl-D-aspartic acid receptor, in mice [30] and has been reported to be associated with human schizophrenia [31]. These observations indicate that the same proteins are involved in mammalian neurogenesis, from ES cells to neural cells, supporting the reliability of the data obtained by proteomic analysis.

In contrast, observations that differ from our data have been reported. For example, proliferating cell nuclear antigen, heterogeneous nuclear ribonucleoprotein K, and peroxiredoxin 4 have been reported to decrease from proliferating human neuronal stem cells (ReNcell VM) to differentiating neuronal stem cells [10]; α-3/α-7 tubulin has been reported to decrease from mouse ES cells to neurons [9]; and translationally controlled tumor protein decreases, but tubulinα-6 and actin-related protein 3 increase, from mouse ES cells to neurons [7]. In addition, although Hsp84 has been reported to increase from adult rat hippocampus NS cells to neurons [6], heat shock protein 90 beta/Hsp84 decreased from NS cells to neurons in monkeys but decreased from ES cells to NS cells in mice [8]. These discrepancies may be due to differences in the origin of the cell lines, cell homogeneity, culture conditions used, and developmental stages of differentiation from ES cells to neurons. Moreover, the competency of NS cells has been reported to change over time during development [35–38].

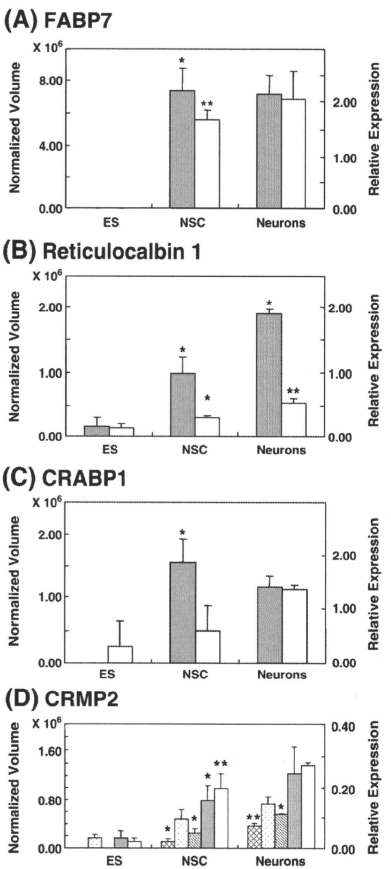

Fig. 3. Protein and RNA expression of five identified genes. RNA expression assayed by real-time RT-PCR and protein expression assayed by 2-DE are plotted for each stage of differentiation (ES cells, NS cells, and neurons). (A–C) White bars indicate RNA expression, whereas gray bars indicate protein expression. (D) White bars refer to RNA expression; gray, slanted stripes, dotted, and checked bars refer to the expression of the proteins CRMP2-1, CRMP2-2, CRMP2-3, and CRMP2-4, respectively. The vertical axis on the left shows the normalized volume of each protein spot on 2-DE, and that on the right shows the relative amounts of RNA normalized with respect to signals from ubiquitously expressed GAPDH mRNA. ES, ES cells; NSC, NS cells. "*" and "**" indicate the *P*-values of 0.05 and 0.01, respectively, for comparisons of the corresponding expression at two stages.

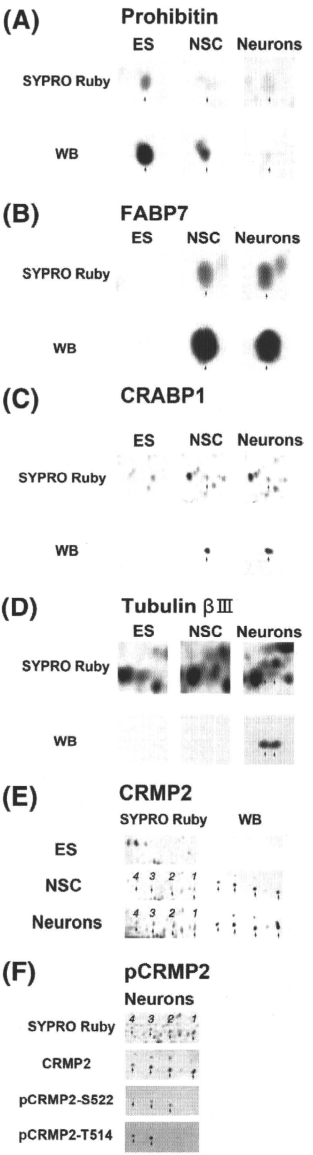

Fig. 4. Two-dimensional Western blotting analysis of a typical enlarged portion from two-dimensional gel electrophoretic gel from ES cells, NS cells, and Neurons. Proteins were visualized by staining with SYPRO Ruby, and by Western blotting analysis with the following antibodies: (A) anti-prohibitin, (B) anti-FABP7, (C) anti-CRABP1, (D) anti-tubulin beta III, (E) anti-CRMP2, and (F) anti-CRMP2 (CRMP2), anti-CRMP2 phosphorylated on Ser-522 (pCRMP2-S522), anti-CRMP2 phosphorylated on Thr-514 (pCRMP2-T514), to detect phosphorylated CRMP2 (pCRMP2). Western blotting analysis of 2-DE gels was performed as described in Materials and methods. ES, ES cells; NSC, NS cells.

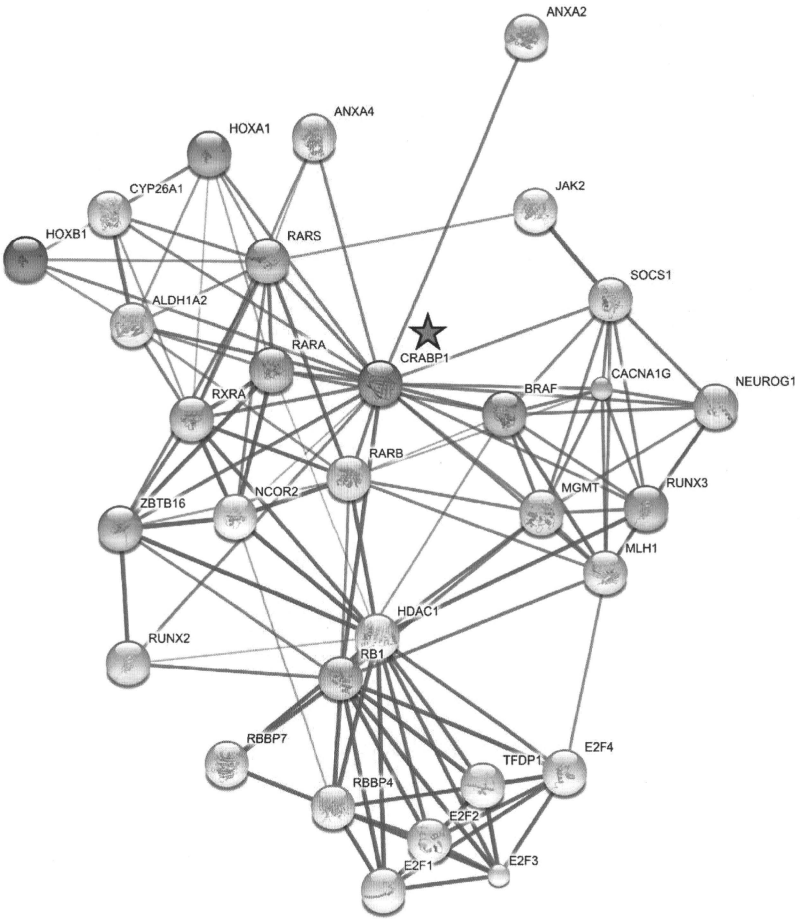

Fig. 5. The protein–protein interaction network of CRABP1. The interaction network was extracted using search tool STRING (http://string.embl.de/).

We found that the expression of galectin 1 and laminin receptor was not altered from monkey ES cells to neural cells, whereas galectin 1 has been found to be increased in mouse NS cells, while both galectin 1and laminin receptor have been reported to decrease in mouse neurons [8]. Prohibitin decreased in monkey NS cells and neurons, in contrast to its upregulation during mouse neural differentiation from ES cells to NS cells [8,34]. The protein–protein interaction network of prohibitin, which was extracted using search tool STRING (http://string.embl.de/) based on reported protein interactions, suggested that mouse and human prohibitins differed in their protein–protein interactions (Supplementary Fig. 1, A and B). Accordingly, the discrepancy between prohibitin expression during neural differentiation from ES cells of mouse and monkey origin may be due to differences in the mechanisms to regulate prohibitin expression via the protein–protein interactions.

Among the newly identified proteins showing increased expression from ES cells to NS cells and neurons were peroxiredoxin 2, CRMP2, and CRABP1, all of which are related to nervous system disorders. For example, the level of the oxidized form of peroxiredoxin 2 has been found to increase in individuals with Alzheimer's disease [39]. It has been reported that CRMP2 is a risk factor of schizophrenia [40], and its hyperphosphorylation is an early event in Alzheimer's disease progression [41].

CRMP2 has been found to bind directly to kinesin light chain and tubulin, resulting in a trimeric complex that stimulates tubulin transport to the distal part of the growing axon [42]. The interaction

between CRMP2 and tubulin has been reported to be altered by CRMP2 phosphorylation, by Cdk5 at Ser^{522} and by GSK-3β at Thr^{514}, inhibiting axon outgrowth [43]. Cdk5 has been reported to be activated in neurons [44] and may play important roles in neurite outgrowth [45] and neuron migration [46]. GSK-3β has been reported to be activated via the activation of Cdk5 as a priming kinase [47]. These findings supported our observation that CRMP2-1 (non-phosphorylated CRMP2) was upregulated in NS cells, and that CRMP2-2 (CRMP2 mono-phosphorylated on Ser522), CRMP2-3 (CRMP2 di-phosphorylated on Ser522 and Thr514), and CRMP2-4 (CRMP2 probably tri-phosphorylated on Ser522, Thr514, and X) were upregulated in NS cells and neurons.

All-trans retinoic acid is used extensively to promote neurogenesis in vitro [7,11,48]. CRABP1 is thought to facilitate catabolism and/or sequestering of retinoic acid, rendering it unavailable to nuclear receptors [32]. Moreover, CRABP2 has been reported to facilitate the transfer of all-trans retinoic acid to the nuclear envelope, where it can interact with its specific receptors. These receptors undergo conformational changes upon ligand binding, allowing the subsequent binding of retinoic acid response elements in certain target genes and their activation [48]. We found that protein expression of CRABP1 was upregulated in NS cells and neurons although its mRNA expression level was unchanged. In NS cells and neurons, however, the level of CRABP2 protein was not altered, although its mRNA expression was downregulated (Supplementary Table 2). The recent finding that CRABP1 is upregulated in human ES cell-derived neuroectodermal spheres bearing neuroprogenitors [11] supports our observations. Taken together, our results suggest that the retinoic acid concentrations and gene activation are tightly regulated during neural differentiation from ES cells. This is interesting, because the practicality of NS cells derived from ES cells may be limited by the teratogenic potential caused by retinoic acid. Retinoic acid concentrations have been reported to be regulated differently under various culture conditions, including in NS cells prepared via ectodermal cells in embryoid bodies [49,50], in the absence of embryoid bodies, by culturing ES cells on mouse-cultured stroma cells [51], or in chemically defined low-density cultures.

Protein interactions of the differentially expressed proteins were explored using STRING (http://string.embl.de/) based on reported protein interactions. As shown in Fig. 5, the interaction map suggested CRABP1 as a date hub, which connects modules as regulators, mediators, or adaptors [52], as well as FABP7, peroxiredoxin 2, and CRMP2 (Supplementary Fig. 1C–E). And the interaction maps suggested Rho GDP dissociation inhibitor 1 and 14-3-3 protein zeta/delta as party hubs, which are involved in signal transduction (Supplementary Fig. 1F and G). Additional studies are needed to elucidate the importance of the specific date hub proteins suggested here.

These results clearly showed that the proteomic approach used here is useful for gaining insight into the molecular mechanism of differentiation and induction from monkey ES cells to NS cells via NSS, and from NS cells to neurons. Together with our previous findings [8], the results presented here suggest that neural differentiation in monkeys is regulated in a manner similar to, but somewhat different from, that in mice, and that higher neural differentiation in monkeys is regulated by more proteins than in mice. In addition, our results provide further evidence that the NSS method we have for the differentiation and induction from monkey ES cells to NS cells and neurons in vitro is useful in providing an experimental model of primate neurogenesis from ES cells to neural cells. Furthermore, our findings indicate that NS cells and neurons differentiated from ES cells by the NSS method may also be useful for fast and effective high throughput drug screening for primate neural diseases.

Further application of proteomics to the detailed stages of differentiation may provide a more complete picture of early primate neurogenesis and enable us to elucidate the differences in characteristics of primate fetal and adult NS cells and neurons.

Conclusion

Using highly homogeneous monkey cells differentiated from ES cells via the formation of NSS, we identified 17 proteins with increased expression and seven with decreased expression from ES cells to NS cells, and three proteins with increased expression and 10 with decreased expression in going from NS cells to neurons. Particularly, FABP7 and CRABP1 were upregulated in NS cells, and CRMP2 was upregulated in NS cells and neurons. FABP7 and CRMP2 mRNAs were also upregulated in NS cells, while CRABP1 mRNA was unchanged. These results provide insight into the molecular basis of monkey neural differentiation.

Supplementary materials related to this article can be found online at doi: 10.1016/j.bbapap.2010.10.009.

Acknowledgments

We are indebted to Professor Takashi Obinata, Dr. Hiroshi Abe, and Dr. Naruki Sato of Chiba University, Japan, for the ultracentrifugal treatment in sample preparation for two-dimensional gel electrophoresis. This work was supported in part by Grant-in-Aid for Scientific Research of Japan and Selective Research Fund of Tokyo Metropolitan University (to N.I.).

References

[1] V.J. Hall, J.Y. Li, P. Brundin, Restorative cell therapy for Parkinson's disease: a quest for perfect cell, Semin. Cell Dev. Biol. 18 (2007) 859–869.
[2] S.V. Liu, iPS cells: a more critical review, Stem Cells Dev. 17 (2008) 391–397.
[3] M. Suzuki, J. McHugh, C. Tork, B. Shelley, S.M. Klein, P. Aebischer, C.N. Svendsen, GDNF secreting human neural progenitor cells protect dying motor neurons, but not their projection to muscle, in a rat model of animal ALS, PLoS ONE 2 (8) (2007) e6891–e68914.
[4] N. Li, H. Sarojini, J. An, E. Wang, Prosaposin in the secretome of marrow stroma-derived neuroprogenitor cells protects neural cells from apoptotic death, J. Neurochem. 112 (2010) 1527–1538.
[5] M. H. Maurer, R.E. Feldmann Jr., C. D. Futterer, W. Kuschinsky, The proteome of neural stem cells from adult rat hippocampus. Proteome Sci. 1 (2003) 1:4.
[6] M.H. Maurer, R.E. Feldmann Jr., C.D. Futterer, J. Butlin, W. Kuschinsky, Comprehensive proteome expression profiling of undifferentiated versus differentiated neural stem cells from adult rat hippocampus, Neurochem. Res. 29 (2004) 1129–1144.
[7] D. Wang, L. Gao, Proteomic analysis of neural differentiation of mouse embryonic stem cells, Proteomics 5 (2005) 4414–4426.
[8] K. Akama, R. Tatsuno, M. Otsu, T. Horikoshi, T. Nakayama, M. Nakamura, T. Toda, N. Inoue, Proteomic identification of differentially expressed genes in mouse neural stem cells and neurons differentiated from embryonic stem cells in vitro, Biochim. Biophys. Acta 1784 (2008) 773–782.
[9] X. Guo, W. Ying, J. Wan, Z. Hu, X. Qian, H. Zhang, F. He, Proteomic characterization of early-stage differentiation of mouse embryonic stem cells into neural cells induced by all-trans retinoic acid in vitro, Electrophoresis 22 (2001) 3067–3075.
[10] R. Hoffrogge, S. Mikkat, C. Scharf, S. Beyer, H. Christoph, J. Pahnke, E. Mix, M. Berth, A. Uhrmacher, I.Z. Zubrzycki, E. Miljan, U. Volker, A. Rolfs, 2-DE proteome analysis of a proliferating and differentiating human neuronal stem cell line (ReNcell VM), Proteomics 6 (2006) 1833–1847.
[11] J.I. Chae, J. Kim, S.M. Woo, H.W. Han, Y.K. Cho, K.B. Oh, K.H. Nam, Y.K. Kang, Cytoskeleton-associated proteins are enriched in human embryonic-stem cell-derived neuroectodermal spheres, Proteomics 9 (2009) 1128–1141.
[12] T. Nakayama, T. Momoki-Soga, N. Inoue, Astrocyte-derived factors instruct differentiation of embryonic stem cells into neurons, Neurosci. Res. 46 (2003) 241–249.
[13] T. Nakayama, T. Momoki-Soga, K. Yamaguchi, N. Inoue, Efficient production of neural stem cells and neurons from embryonic stem cells, NeuroReport 15 (2004) 487–491.
[14] T. Nakayama, T. Sai, M. Otsu, T. Momoki-Soga, N. Inoue, Astrocytogenesis of embryonic stem-cell-derived neural stem cells: Default differentiation, NeuroReport 17 (2006) 1519–1523.
[15] S. Muramatsu, T. Okuno, Y. Suzuki, T. Nakayama, T. Kakiuchi, N. Takino, A. Iida, F. Ono, K. Terao, N. Inoue, I. Nakano, Y. Kondo, H. Tsukada, Multitracer assessment of dopamine function after transplantation of embryonic stem cell-derived neural stem cells in a primate model of Parkinson's disease, Synapse 63 (2009) 541–548.
[16] H. Suemori, T. Tada, R. Torii, Y. Hosoi, K. Kobayashi, H. Imahie, Y. Kondo, A. Iritani, N. Nakatsuji, Establishment of embryonic stem cell lines from cynomolgus monkey blastocysts produced by IVF or ICSI, Dev. Dyn. 222 (2001) 273–279.
[17] T. Toda, N. Kimura, Standardization of protocol for Immobiline 2-D PAGE and construction of 2-D PAGE protein database on World Wide Web home page, Jpn. J. Electrophor. 41 (1997) 13–20.

[18] S. Kaech, H. Parmar, M. Roelandse, C. Bornmann, A. Matus, Cytoskeletal microdifferentiation: a mechanism for organizing morphological plasticity in dendrites, Proc. Natl Acad. Sci. USA 98 (2001) 7086–7092.
[19] T. Sasaki, Y. Takai, The Rho small G protein family-Rho GDI system as a temporal and spatial determinant for cytoskeletal control, Biochem. Biophys. Res. Commun. 245 (1998) 641–645.
[20] J. Wang, H. Lou, C.J. Pedersen, A.D. Smith, R.G. Perez, 14-3-3zeta contributes to tyrosine hydroxylase activity in MN9D cells: localization of dopamine regulatory proteins to mitochondria, J. Biol. Chem. 284 (2009) 14011–14019.
[21] S. Patrakitkomjorn, D. Kobayashi, T. Morikawa, M. Morifuji-Wilson, N. Tsubota, A. Irie, T. Ozawa, M. Aoki, N. Arimura, K. Kaibuchi, H. Saya, N. Araki, Neurofibromatosis type 1 (NF1) tumor suppressor, neurofibromin, regulates the neuronal differentiation of PC12 cells via its associating protein, CRMP-2, J. Biol. Chem. 283 (2008) 9399–9413.
[22] N. Arimura, K. Kaibuchi, Neuronal polarity: from extracellular signals to intracellular mechanisms, Nat. Rev. Neurosci. 8 (2007) 194–205.
[23] L.M. Brill, W. Xing, K.-B. Lee, S.B. Ficarro, A. Crain, Y. Xu, A. Terskikh, E.Y. Snyder, S. Ding, Phosphoproteomic analysis of human embryonic stem cells, Cell Stem Cell 5 (2009) 204–213.
[24] D.V. Hoof, J. Munoz, S.R. Braam, M.W.H. Pinkse, R. Linding, A.J.R. Heck, C.L. Mummery, J. Krijgsveld, Phosphorylation dynamics during early differentiation of human embryonic stem cells, Cell Stem Cell 5 (2009) 214–226.
[25] S.J. Ullrich, E.A. Robinson, L.W. Law, M. Willingham, E. Appella, A mouse tumor-specific transplantation antigen is a heat shock-related protein, Proc. Natl Acad. Sci. USA 83 (1986) 3121–3125.
[26] S. Ichimiya, J.G. Davis, D.M. O'Rourke, M. Katsumata, M.I. Greene, Murine thioredoxin peroxidase delays neuronal apoptosis and is expressed in areas of the brain most susceptible to hypoxic and ischemic injury, DNA Cell Biol. 16 (1997) 311–321.
[27] Y. Arai, N. Funatsu, K. Numayama-Tsuruta, T. Nomura, S. Nakamura, N. Osumi, Role of Fabp7, a downstream gene of Pax6, in the maintenance of neuroepithelial cells during early embryonic development of the rat cortex, J. Neurosci. 25 (2005) 9752–9761.
[28] T.E. Anthony, C. Klein, G. Fishell, N. Heintz, Radial glia serve as neuronal progenitors on all regions of the central nervous system, Neuron 41 (2004) 881–890.
[29] Y. Owada, T. Yoshimoto, H. Kondo, Spatio-temporally differential expression of genes for three members of fatty acid binding proteins in developing and mature rat brains, J. Chem. Neuroanat. 12 (1996) 113–122.
[30] Y. Owada, S.A. Abdelwahab, N. Kitanaka, H. Sakagami, H. Takano, Y. Sugitani, M. Sugawara, H. Kawashima, Y. Kiso, J.I. Mobarakeh, K. Yanai, K. Kaneko, H. Sasaki, H. Kato, S. Saino-Saito, N. Matsumoto, N. Akaike, T. Noda, H. Kondo, Altered emotional behavioral responses in mice lacking brain-type fatty acid-binding protein gene, Eur. J. Neurosci. 24 (2006) 175–187.
[31] A. Watanabe, T. Toyota, Y. Owada, T. Hayashi, Y. Iwayama, M. Matsumata, Y. Ishitsuka, A. Nakaya, M. Maekawa, T. Ohnishi, R. Arai, K. Sakurai, K. Yamada, H. Kondo, K. Hashimoto, N. Osumi, T. Yoshikawa, Fabp7 maps to a quantitative trait locus for a schizophrenia endophenotype, PLoS Biol. 5 (2007) e297:1–15.
[32] D. Dong, S.E. Ruuska, D.J. Levinthal, N. Noy, Distinct roles for cellular retinoic acid-binding proteins I and II in regulating signaling by retinoic acid, J. Biol. Chem. 274 (1999) 23695–23698.
[33] S.A. Ross, P.J. McCaffery, U.C. Drager, L.M. De Luca, Retinoids in embryonal development, Physiol. Rev. 80 (2000) 1021–1054.
[34] A. Battersby, R.D. Jones, K.S. Lilley, R.J. McFarlane, H.R. Braig, N.D. Allen, J.A. Wakeman, Comparative proteomic analysis reveals differential expression of Hsp25 following the directed differentiation of mouse embryonic stem cells, Biochim. Biophys. Acta 1773 (2007) 147–156.
[35] S.K. McConnell, Constructing the cerebral cortex: neurogenesis and fate determination, Neuron 15 (1995) 761–768.
[36] X. Qian, Q. Shen, S.K. Goderie, W. He, A. Capela, A.A. Davis, S. Temple, Timing of CNS cell generation: a programmed sequence of neuron and glial cell production from isolated murine cortical stem cells, Neuron 28 (2000) 69–80.
[37] S. Temple, The development of neural stem cells, Nature 414 (2001) 112–117.
[38] J. Hatakeyama, Y. Bessho, K. Katoh, S. Ookawara, M. Fujioka, F. Guillemot, R. Kageyama, Hes genes regulate size, shape and histogenesis of the nervous system by control of the timing of neural stem cell differentiation, Development 131 (2006) 5539–5550.
[39] Y. Yoshida, A. Yoshikawa, T. Kinumi, Y. Ogawa, Y. Saito, K. Ohara, H. Yamamoto, Y. Imai, E. Niki, Hydroxyoctadecadienoic acid and oxidatively modified peroxiredoxins in the blood of Alzheimer's disease patients and their potential as biomarkers, Neurobiol. Aging 30 (2009) 174–185.
[40] K. Nakata, H. Ujike, A. Sakai, M. Takaki, T. Imamura, Y. Tanaka, S. Kuroda, The human dihydropyrimidinase-related protein 2 gene on chromosome 8p21 is associated with paranoid-type schizophrenia, Biol. Psychiatry 53 (2003) 571–576.
[41] A.R. Cole, W. Noble, L. van Aalten, F. Plattner, R. Meimaridou, D. Hogan, M. Taylor, J. LaFrancois, F. Gunn-Moore, A. Verkhratsky, S. Oddo, F. LaFerla, K.P. Giese, K.T. Dineley, K. Duff, J.C. Richardson, S.D. Yan, D.P. Hanger, S.M. Allan, C. Sutherland, Collapsin response mediator protein-2 hyperphosphorylation is an early event in Alzheimer's disease progression, J. Neurochem. 103 (2007) 1132–1144.
[42] T. Kimura, H. Watanabe, A. Iwamatsu, K. Kaibuchi, Tubulin and CRMP-2 complex is transported via Kinesin-1, J. Neurochem. 93 (2005) 1371–1382.
[43] T. Yoshimura, Y. Kawano, N. Arimura, S. Kawabata, A. Kikuchi, K. Kaibuchi, GSK-3beta regulates phosphorylation of CRMP-2 and neuronal polarity, Cell 120 (2005) 137–149.
[44] J. Lew, Q.Q. Huang, Z. Qi, R.J. Winkfein, R. Aebersold, T. Hunt, J.H. Wang, A brain-specific activator of cyclin-dependent kinase 5, Nature 371 (1994) 423–426.
[45] M. Nikolic, H. Dudek, Y.T. Kwon, Y.F. Ramos, L.H. Tsai, The cdk5/p35 kinase is essential for neurite outgrowth during neuronal differentiation, Genes Dev. 10 (1996) 816–825.
[46] T. Chae, Y.T. Kwon, R. Bronson, P. Dikkes, E. Li, L.H. Tsai, Mice lacking p35, a neuronal specific activator of Cdk5, display cortical lamination defects, seizures, and adult lethality, Neuron 18 (1997) 29–42.
[47] A.R. Cole, F. Causeret, G. Yadirgi, C.J. Hastie, H. McLauchlan, E.J. McManus, F. Hernandez, B.J. Eickholt, M. Nikolic, C. Sutherland, Distinct priming kinases contribute to differential regulation of collapsin response mediator proteins by glycogen synthase kinase-3 in vivo, J. Biol. Chem. 281 (2006) 16591–16598.
[48] A. Budhu, R. Gillilan, N. Noy, Localization of the RAR interaction domain of cellular retinoic acid binding protein-II, J. Mol. Biol. 305 (2001) 939–949.
[49] G. Bain, D. Kitchens, M. Yao, J.E. Huettner, D.I. Gottlieb, Embryonic stem cells express neuronal properties in vitro, Dev. Biol. 168 (1995) 342–357.
[50] S. Okabe, K. Forsberg-Nilsson, A.C. Spiro, M. Segal, R.D. McKay, Development of neuronal precursor cells and functional postmitotic neurons from embryonic stem cells in vitro, Mech. Dev. 59 (1996) 89–102.
[51] H. Kawasaki, K. Mizuseki, S. Nishikawa, S. Kaneko, Y. Kuwana, S. Nakanishi, S.I. Nishikawa, Y. Sasai, Induction of midbrain dopaminergic neurons from ES cells by stromal cell-derived inducing activity, Neuron 28 (2000) 31–40.
[52] J.-D.J. Han, N. Bertin, T. Hao, D.S. Goldberg, G.F. Berriz, L.V. Zhang, D. Dupuy, A.J.M. Walhout, M.E. Cusick, F.P. Roth, M. Vidal, Evidence for dynamically organized modularity in the yeast protein–protein interaction network, Nature 430 (2004) 88–93.

JOURNAL OF PROTEOMICS 74 (2011) 431–441

available at www.sciencedirect.com

ScienceDirect

www.elsevier.com/locate/jprot

N^{α}-Acetylation of yeast ribosomal proteins and its effect on protein synthesis

Masahiro Kamita[a], *Yayoi Kimura*[a], *Yoko Ino*[a], *Roza M. Kamp*[b], *Bogdan Polevoda*[c], *Fred Sherman*[c], *Hisashi Hirano*[a,*]

[a]*Graduate School of Nanobioscience, Yokohama City University, Suehiro 1-7-29, Tsurumi, Yokohama 230-0045, Japan*
[b]*University of Applied Science and Technology, 13347 Berlin, Germany*
[c]*Department of Biochemistry and Biophysics, University of Rochester Medical Center, Rochester, NY 14642, USA*

ARTICLE INFO

Article history:
Received 21 November 2010
Accepted 15 December 2010
Available online 22 December 2010

Keywords:
N^{α}-Acetylation
Ribosome
Ribosomal protein
2D-DIGE

ABSTRACT

N^{α}-Acetyltransferases (NATs) cause the N^{α}-acetylation of the majority of eukaryotic proteins during their translation, although the functions of this modification have been largely unexplored. In yeast (*Saccharomyces cerevisiae*), four NATs have been identified: NatA, NatB, NatC, and NatD. In this study, the N^{α}-acetylation status of ribosomal protein was analyzed using NAT mutants combined with two-dimensional difference gel electrophoresis (2D-DIGE) and mass spectrometry (MS). A total of 60 ribosomal proteins were identified, of which 17 were N^{α}-acetylated by NatA, and two by NatB. The N^{α}-acetylation of two of these, S17 and L23, by NatA was not previously observed. Furthermore, we tested the effect of ribosomal protein N^{α}-acetylation on protein synthesis using the purified ribosomes from each NAT mutant. It was found that the protein synthesis activities of ribosomes from NatA and NatB mutants were decreased by 27% and 23%, respectively, as compared to that of the normal strain. Furthermore, we have shown that ribosomal protein N^{α}-acetylation by NatA influences translational fidelity in the presence of paromomycin. These results suggest that ribosomal protein N^{α}-acetylation is necessary to maintain the ribosome's protein synthesis function.

1. Introduction

Methionine cleavage and N^{α}-acetylation are two common protein N-terminal modifications [1,2]. A majority of experimentally characterized eukaryotic proteins are N-terminally acetylated by N^{α}-acetyltransferases (NATs) during their translation from mRNA [3]. In yeast (*Saccharomyces cerevisiae*), approximately 57% of proteins are predicted to have an N^{α}-acetyl group, while the corresponding figure for mammalian proteins is about 84% [4]. The N^{α}-acetylation is catalyzed by NATs that contain catalytic subunits homologous to the GNAT family of acetyltransferase [5]. In yeast, four NATs have been identified, NatA, NatB, NatC, and NatD, which are composed of the following catalytic and auxiliary subunits: Ard1p and Nat1p for NatA; Nat3p and Mdm20p for NatB; and Mak3p, Mak10p, and Mak31p for NatC [6]. A recent study has shown NatD to consist of only a catalytic subunit: Nat4p [7]. The deletion of NATs induces various phenotypes. The NatA deletion mutant exhibits defects in sporulation, salt sensitivity, mating efficiency, and the ability to enter G0. The NatB deletion mutant shows increased osmotic sensitivity, decreased utilization of non-fermentable carbon sources, reduced mating efficiency, inability to form functional actin filaments, defects in mitochondrial and vacuolar inheritance, random polarity, increased sensitivity to the anti-mitotic drugs, and increased susceptibility to a number of DNA damaging agents. The NatC deletion mutant shows a decreased growth on YPG medium at 37 °C, although growth on YPD medium at 30 °C is nearly normal [6].

* *Corresponding author.* Tel.: +81 45 508 7439; fax: +81 45 508 7667.
E-mail address: hirano@yokohama-cu.ac.jp (H. Hirano).

1874-3919/$ – see front matter
doi:10.1016/j.jprot.2010.12.007

Despite the wide occurrence of protein N^{α}-acetylation, it is unknown how many proteins require N^{α}-acetylation for function. For instance, the N^{α}-acetylation of Orc1p and Sir3p was shown to be necessary for transcriptional silencing in yeast [8,9]. Also, the N^{α}-acetylation of the killer viral coat protein Gag by NatC is required for assembly and maintenance of the L-A dsRNA viral particle in yeast [10]. Unacetylated actin and tropomyosin have a number of defects *in vivo* and *in vitro*, although the mutants are viable [11]. While the N^{α}-acetylation of ribosomal proteins has been known for decades [12–14], the role of N^{α}-acetylation in translation has not been determined.

The ribosome is a large ribonucleoprotein complex that synthesizes proteins in the cytoplasm. The core of the structure, as well as many of the ribosomal functions, is highly conserved between eukaryotes and prokaryotes [15]. In yeast, the ribosome consists of two subunits, the large (60S) and small (40S) subunits. The 60S subunit is composed of three ribosomal RNAs (rRNAs) and 46 ribosomal proteins, whereas the 40S subunit is composed of one rRNA and 32 ribosomal proteins [16,17]. The ribosome translates mRNA sequences into the corresponding amino acids and links them together to synthesize proteins. There are four stages of protein synthesis: initiation, elongation, termination, and recycling [18]. The 60S subunit polymerizes the polypeptide chain during the elongation phase. The 40S subunit is associated with mRNA tracks, the tRNA binding site, and is instrumental in selecting an aminoacyl-tRNA that complements the bound mRNA codon [16]. Although the rRNAs basically catalyze translation of mRNA and peptide bond formation, ribosomal proteins have been shown to play several important roles in protein synthesis, including determining the conformation of the ribosome structure and binding the various translational factors [19].

The ribosomal proteins undergo a variety of post-translational modifications including phosphorylation, methylation, glycosylation, and N^{α}-acetylation (co-translational). The post-translational modifications are thought to affect the ribosomal function. For example, Ruvinsky et al. reported that phosphorylation of ribosomal protein S6 controls cell size and glucose homeostasis [20]. Phosphorylation of ribosomal protein P1A exerts an effect on the heterooligomerization process [21]. Additionally, it is known that arginine methylation of ribosomal protein S10 regulates ribosome biogenesis [22], and arginine methylation of ribosomal proteins S3 affects ribosome assembly [23]. Glycosylation of ribosomal proteins is required for aggregation of untranslated messenger ribonucleoproteins into stress granules [24]. Clearly, modifications of ribosomal proteins are important for protein synthesis. However, the effect of N^{α}-acetylation of ribosomal proteins, and therefore changes of ribosome function remain unknown.

In this study, we comprehensively analyzed ribosomal protein N^{α}-acetylation using NAT mutants combined with two-dimensional difference gel electrophoresis (2D-DIGE) and mass spectrometry (MS). These analyses led to the identification of 19 ribosomal proteins acetylated by NatA and NatB. Subsequently, we investigated the effect of ribosomal protein N^{α}-acetylation on protein synthesis using the NatA deletion mutant.

2. Material and methods

2.1. *Yeast strains and media*

The following strains were used in this study: the normal strain, B-8032 (*MATα ura3-52 CYC1-963 cyc7-67 lys5-10*); the *nat1* mutant, B-8360 (*MATα nat1::URA3 ura3-52 CYC1-963 cyc7-67 lys5-10*); the *mak3* mutant, B-9074 (*MATα mak3::URA3 CYC1-963 cyc7-67 lys5-10*); and the *nat3* mutant, B-11974 (*MATα nat3::kanMX2 CYC1-963 cyc7-67 lys5-10*).

The YPD medium [2% (w/v) glucose, 2% (w/v) pepton, and 1% (w/v) yeast extract] was used for growing yeast. To purify 80S ribosomes, the yeast cells were cultured in the YPD medium at 30 °C. The cells were grown to the mid log phase, an absorbance of ~2 A_{600}U/ml, and harvested by centrifugation, washed once with deionized water and stored at −80 °C. For the 10-fold serial dilution assays, freshly grown yeast colonies were suspended in deionized water, and 1/10 dilutions, starting at an optical density of 0.1 at 600 nm, were spotted on a YPD plate or a YPD plate containing antibiotics. The plates were then incubated at 20, 30, or 37 °C for 3 to 4 days.

2.2. *Purification of 80S ribosomes and ribosomal proteins*

Purification of yeast ribosomes was performed as described by Ulrich A et al. with some modifications [25]. Briefly, the stored yeast cells were resuspended in the extraction buffer [20 mM HEPES-KOH pH 7.0, containing 5 mM Mg-acetate$_2$, 2 mM spermidine, 0.1 mM EGTA, 10 mM 2-mercaptoethanol, 10% (v/v) glycerol, and 0.1 mM PMSF]. Glass beads were added and the cells broken by vigorous vortex shaking. The homogenate was centrifuged at 20,000 ×*g* for 30 min at 4 °C. To purify 80S ribosomes, the concentration of KCl in the supernatant was adjusted to 0.4 M while being mixed gently. Thereafter, the supernatant was centrifuged at 65,000 ×*g* for 5 h at 4 °C. The resulting ribosome pellet was then resuspended in the dissociation buffer [20 mM HEPES-KOH pH 7.0, containing 5 mM Mg-(Ac)$_2$, 500 mM K(Ac), 0.1 mM EGTA, 10 mM 2-mercaptoethanol, 10% (v/v) glycerol, and 0.1 mM PMSF] and puromycin and GTP were added to a final concentration of 1 mM each. The mixture was incubated at 30 °C for 30 min. After incubation, the ribosome was pelleted through a 25% (v/v) glycerol cushion in the dissociation buffer at 65,000 ×*g* for 12 h at 4 °C using a swinging bucket rotor. The pellet was resuspended again and then centrifuged at 65,000 ×*g* for 12 h at 4 °C. Finally, the resulting 80S ribosome pellet was resuspended in the reaction buffer [50 mM Tris–HCl pH 7.6 containing 15 mM $MgCl_2$, and 90 mM KCl]. To separate the ribosomal proteins from the rRNA of the ribosome, the resuspended pellet was precipitated with 0.1 volume of 0.1% (w/v) DTT, 0.1 volume of 1 M $MgCl_2$, and 2.5 volume of glacial acetic acid. After incubation on ice for 1 h, the rRNA was removed by centrifugation at 20,000 ×*g* for 10 min. The supernatant was dialyzed against deionized water.

2.3. *Gel electrophoresis of rRNAs and ribosomal proteins*

The rRNAs (1 μg) were incubated at 65 °C for 2 min in the loading solution [0.1% (w/v) SDS, 5% (v/v) glycerol and BPB],

and subjected to electrophoresis in 0.8% (w/v) agarose gel. The ribosomal proteins (10 μg) were incubated at 65 °C for 10 min in the sample buffer [0.05 M Tris–HCl pH 6.8, containing 2% (w/v) SDS, 5% (v/v) 2-mercaptoethanol, 10% (v/v) glycerol, and BPB] and subsequently separated by SDS-PAGE. On the other hand, two-dimensional electrophoresis (2-DE) was performed using acid-urea gels containing 8 M urea in the first dimension toward the cathode (pH 5.0) at constant 200 V for 800 Vh, and SDS-PAGE (14% acrylamide gel) in the second dimension. After 2-DE, proteins were detected by CBB R-250 staining.

2.4. *Two-dimensional difference gel electrophoresis*

For 2D-DIGE, purified ribosomal proteins were minimally labeled with CyDyes (GE Healthcare, Little Calfont, UK) Cy3 and Cy5 according to the manufacturer's protocol. Equal amounts of purified ribosomal proteins from the normal and the mutant strains were labeled with two different dyes, Cy3 for the normal and Cy5 for the mutant strains. The ratio of ribosomal proteins to CyDye was 50 μg to 128 pmol. All labeled samples were combined and dissolved in 20 μl of sample solution [10% (v/v) 2-mercaptoethanol, 10% (v/v) glycerol, 1% (v/v) acetic acid and 8 M urea], and was subjected to 2-DE. The separated proteins were detected using Typhoon 9400 (GE Healthcare).

2.5. *Protein identification by mass spectrometric analysis*

After electrophoresis, protein spots were cut from the gels, destained three times with destaining solution [50 mM NH_4HCO_3/60% ACN], and digested with trypsin in 50 mM NH_4HCO_3 at 37 °C for 12 h. The tryptic digests were applied to Amicon Ultrafree-MC (0.22 μm) devices and centrifuged at 7000 rpm for 5 min. After filtration, a solution containing 0.02% (v/v) TFA and 0.2% (v/v) formic acid was added to the Amicon Ultrafree-MC tubes and centrifuged again. The resulting peptides were resuspended in 0.3% (v/v) formic acid, and analyzed using an ESI-Linear Ion Trap (LIT)-TOF MS (NanoFrontier LD, Hitachi-High Technologies, Tokyo, Japan) or an ESI-Q-TOF MS (Micromass, Manchester, UK), respectively. For data analysis, the raw MS spectrum was processed using the Hitachi-High Technologies' data processing software or the Micromass' MassLynx software to generate MGF and PKL files, respectively. The obtained MS and MS/MS data were searched against the 6,858 yeast protein sequences of the SWISS-PROT ver. 57.4 database using the MASCOT program, ver. 2.2.04 (Matrix Science, London, UK) to identify proteins. The search parameters were as follows: protease digestion with two missed cleavages permitted, enzyme specificity was set to consider trypsin, propionamidation of cysteine, and oxdation of methionine as variable modifications, and mass tolerance was set to 0.5 Da for the fragment ions and precursor ions. The confidence interval for the MASCOT scores was set to 95% (significance threshold $p<0.05$). Additionally, search results that yielded a MASCOT score of ≥95 or 35 for SDS-PAGE or 2-DE, respectively, were accepted as positive identifications.

2.6. *Poly (U)-dependent poly (Phe) synthesis assay*

The 80S ribosomes (0.3 A_{260}U) from the normal and the mutant strains were incubated in 25 μl of an assay mixture containing 50 μg of S-100 fraction, which was purified from the normal strain, 15 μg of polyuridylic acid, 25 μg of tRNA, [^{14}C]-phenylalanine, 0.5 mM GTP, 1 mM ATP, 2 mM phosphocreatine, and 40 μg/ml creatine phosphokinase in 50 mM Tris–HCl pH 7.6, 15 mM $MgCl_2$, 90 mM KCl, and 5 mM 2-mercaptoethanol at 30 °C for 30 min. After incubation, samples were precipitated with 10% (w/v) trichloroacetic acid (TCA) and boiled for 10 min. Subsequently, the samples were placed on ice for 10 min and filtered through glass fiber filters. The filters were washed twice with 10% (w/v) TCA. After air-drying, the insoluble proteins were resuspended in 10% (w/v) TCA and the radioactivity was measured using a liquid scintillation counter.

2.7. *Polysome profiles*

Yeast cells were grown to a mid log phase in the YPD medium. The cells were harvested in the presence of 100 μg/ml cycloheximide for 10 min. Preparation of yeast extracts was carried out by glass bead disruption in 10 mM Tris–HCl pH 7.4, containing 100 mM NaCl, 30 mM $MgCl_2$, and 100 μg/ml cycloheximide. A 200 μl sample of lysate, corresponding to 8 A_{260} U, was applied to a 7–47% linear sucrose gradient that was prepared in 50 mM Tris–acetate pH 7.0, containing 50 mM NH_4Cl, 30 mM $MgCl_2$ and 1 mM DTT for 2.5 h at 38,200 rpm (Beckman, SW40Ti). After centrifugation, fractions were collected from top to bottom with continuous A_{254} monitoring.

2.8. *Translational fidelity assay*

The reporter assay described by Liang et al. was performed with slight modifications [26]. Briefly, a 366 bp PCR fragment containing the Protein A gene was amplified from the common TAP tag. To create the gene encoding the FLAG tag, which is immediately downstream from the stop codon gene of protein A, the first PCR fragment was used as a template for the second PCR. The created PCR fragment was inserted into the KpnI and XbaI restriction site in the plasmid pAUR123. The construct was transformed into both the normal strain and the *nat1* mutant. The transformed cells were disrupted using YPER buffer (Pierce, Rockford, IL, USA) and glass beads. Cell extracts were centrifuged at 20,000 ×g for 10 min at 4 °C and supernatants analyzed by SDS-PAGE. The separated proteins were transferred to a polyvinylidene difluoride (PVDF) membrane and the protein A peptide on the membrane was detected with anti-peroxidase antibody. The membrane was incubated with ECL plus (GE Healthcare) and the positive signals were detected using an LAS4000 illuminator (Fuji Film, Tokyo, Japan).

3. Results

3.1. *Ribosome purification and ribosomal protein identification by two-dimensional electrophoresis*

In this study, we purified the 80S ribosomes from the normal yeast strain and the NAT mutants. To check the quality of the purified 80S ribosomes, rRNAs and ribosomal proteins were separated by standard gel electrophoresis (Fig. 1A). As shown in Fig. 1A, sharp bands of 25S and 18S rRNAs were detected, while no

smeared band was detected; this shows that intact 80S ribosomes were purified, with no degradation incurred during purification. Simultaneously, the ribosomal proteins of the 80S ribosomes from the normal strain and the NAT mutants were separated by SDS-PAGE and detected by CBB staining (Fig. 1B). It should be noted that CBB-stained ribosomal protein gel images from the normal strain and the NAT mutants were identical. Then, gel-separated protein bands were in gel-digested by trypsin and the resulting peptides were analyzed by MS/MS to identify the proteins (Supplementary Table 1). A total of 50 ribosomal proteins were identified, but no non-ribosomal proteins were found, indicating that the ribosomes were highly purified.

Next, the ribosomal proteins were separated using 2-DE and detected by CBB staining (Fig. 1C). A total of 59 protein spots were detected on the 2-DE gel. These proteins were in gel-digested with trypsin, and the resultant peptides were analyzed by MS/MS to identify 60 ribosomal proteins (Fig. 1C and Supplementary Table 2). Interestingly, ribosomal proteins S5 (spots 5 and 6) and S10 (spots 54, 55, and 56) were identified in more than two spots having different isoelectric points, suggesting that these ribosomal proteins may be modified with a modification group such as phosphate.

3.2. *Identification of N$^{\alpha}$-acetylated ribosomal proteins*

To identify which of the NATs acetylates which ribosomal proteins, we analyzed the ribosomal proteins in the normal strain and the NAT mutants using 2D-DIGE, and found that

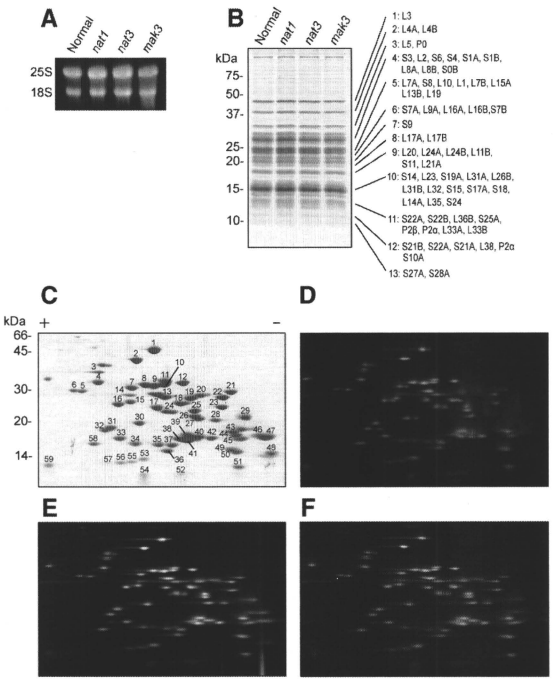

Fig. 1 – Analysis of rRNAs and N$^{\alpha}$-acetylated ribosomal proteins by 2D-DIGE. (A) Purified rRNA from yeast 80S ribosomes was separated by agarose gel electrophoresis and stained with ethidium bromide. (B) Purified ribosomal proteins from yeast 80S ribosomes were separated by SDS-PAGE and stained with CBB R-250. The details of MS data using an ESI-LIT-TOF MS was shown in Supplementary Table 1. (C) Purified ribosomal proteins from yeast 80S ribosomes were separated by 2-DE using acid-urea electrophoresis in the first dimension and SDS-PAGE in the second dimension and stained with CBB R-250. Protein spots identified by an ESI-Q-TOF-MS are numbered and their details were indicated in Supplementary Table 2. (D–F) Identification of the N$^{\alpha}$-acetylated ribosomal proteins from the *nat1*, *nat3*, and *mak3* mutants, respectively. Equal amounts of purified ribosomal proteins from the normal strain and the NAT mutant were labeled with Cy3 and Cy5 respectively. The Cy-labeled ribosomal proteins from the two strains were separated on the same 2-DE gel and the Cy3- and Cy5-images were compared. The N$^{\alpha}$-acetylated ribosomal proteins are shown in Table 1.

Table 1 – N$^{\alpha}$-Acetylation of ribosomal proteins.

Subunit	Protein	MW (kDa) [a]	pI [a]	2-DE [b]	TOF-MS [c]	DIGE	NAT
60S	P0	33.7	4.6	–	–	–	–
	P1 A/B	10.9/10.6	3.6/3.7	–	●/–	–	–
	P2 A/B	10.7/11.1	3.8/3.9	–	O/O	–	–
	L1 A/B [d]	24.5/24.5	9.7/9.7	–	●/●	●/●	NatA
	L2 A/B [d]	27.4/27.4	11.1/11.1	O/–	–	O/O	–
	L3	43.7	10.3	O	–	O	–
	L4 A/B	39.0/39.0	10.6/10.6	●/–	–	●/●	NatA
	L5	33.7	6.4	–	–	O	–
	L6 A/B	19.9/20.0	10.1/10.1	–	●/–	O/O	–
	L7 A/B	27.6/27.7	10.2/10.2	O/–	O/–	O/O	–
	L8 A/B	28.1/28.1	10.0/10.0	O/–	O/–	O/O	–
	L9 A/B	21.6/21.7	9.7/10.5	–	–	O/–	–
	L10	25.4	10.8	–	O	–	–
	L11 A/B	19.7/19.7	9.9/9.9	●	●/●	●/●	NatA
	L12 A/B [d]	17.8/17.8	9.4/9.4	–	–	O/O	–
	L13 A/B	22.5/22.5	11.2/11.7	–	–	O/–	–
	L14 A/B	15.2/15.2	10.4/11.6	–	●/–	●/–	NatA
	L15 A/B [d]	24.4/24.4	11.4/12.0	O/–	–	O/–	–
	L16 A/B	22.2/22.2	10.5/10.5	●/●	–/●	●/●	NatA
	L17 A/B	20.5/20.5	10.9/10.9	–	O/–	O/O	–
	L18 A/B [d]	20.6/20.6	11.7/11.7	–	–	O/O	–
	L19 A/B [d]	21.7/21.7	11.4/11.4	O/–	–	O/O	–
	L20 A/B	20.4/20.4	10.3/10.3	–	–	O/O	–
	L21 A/B	18.2/18.3	10.4/11.2	–	O/–	O/–	–
	L22 A/B	13.7/13.8	5.9/6.0	–	O/–	O/–	–
	L23 A/B [d]	14.5/14.5	10.3/10.3	–	–	●/●	NatA
	L24 A/B	17.6/17.5	11.3/11.4	–	–	O/O	–
	L25	15.7	10.1	O	O	O	–
	L26 A/B	14.2/14.2	11.4/10.5	–	–/O	–/O	–
	L27 A/B	15.5/15.5	10.4/11.2	–	O/–	O/–	–
	L28	16.7	10.5	–	O	O	–
	L29	6.7	12	–	O	–	–
	L30	11.4	9.8	–	O	O	–
	L31 A/B	12.9/13.0	10.0/10.0	–	O/–	O/O	–
	L32	14.8	11.2	–	O	O	–
	L33 A/B	12.1/12.2	11.1/11.1	–	●/–	O/O	–
	L34 A/B	13.6/13.6	11.6/11.6	–	–	–	–
	L35 A/B [d]	13.9/13.9	10.6/10.6	–	–	O/O	–
	L36 A/B	11.1/11.1	12.2/11.6	–	●/ O	–/O	–
	L37 A/B	9.8/9.7	12.2/12.3	–	–	–	–
	L38	8.8	10.9	–	O	O	–
	L39	6.3	–	–	O	–	–
	L40 A/B [d]	14.5/14.5	10.6/10.6	–	–	–	–
	L41 A/B [d]	3.3/3.3	–	–	–	–	–
	L42 A/B [d]	12.2/12.2	11.4/11.4	–	–/O	–	–
	L43 A/B [d]	10.0/10.0	11.2/11.4	–	–	–	–
40S	S0 A/B	28.0/28.0	4.5/4.5	–	●/–	–	–
	S1 A/B	28.7/28.8	10.0/10.0	●/–	●/–	O/O	NatA
	S2	27.4	10.4	●	●	●	NatA
	S3	26.5	9.4	O	O	O	–
	S4 A/B [d]	29.3/29.3	10.1/10.1	–	O/–	O/O	–
	S5	25	8.6	●	●	●	NatA
	S6 A/B [d]	27.0/27.0	10.4/10.4	–	–	O/O	–
	S7 A/B	21.6/21.6	9.8/9.9	●/–	●/●	●/●	NatA
	S8 A/B [d]	22.5/22.5	10.7/10.7	–	O/–	O/O	–
	S9 A/B	22.4/22.3	10.8/10.1	–	–	–/O	–
	S10 A/B	12.7/12.7	8.7/9.92	–	O/O	O/–	–
	S11 A/B [d]	17.7/17.7	10.8/10.8	–	●/–	●/●	NatA
	S12	15.8	4.5	–	–	–	–
	S13	17	10.4	–	O	O	–
	S14 A/B	14.5/14.6	10.7/11.3	●/–	●/–	●/–	NatA
	S15	16	10.7	–	●	●	NatA
	S16 A/B [d]	15.8/15.8	10.3/10.3	●/–	●/–	●/●	NatA

(continued on next page)

Table 1 (*continued*)

Subunit	Protein	MW (kDa)[a]	pI[a]	2-DE[b]	TOF-MS[c]	DIGE	NAT
40S	S17 A/B	15.8/15.8	10.5/11.3	–	–	●/–	NatA
	S18 A/B[d]	17.0/17.0	10.3/10.3	–	●/●	●/●	NatA
	S19 A/B	15.9/15.9	9.6/10.5	–	–/O	O/–	–
	S20	13.9	9.5	–	●	●	NatA
	S21 A/B	9.7/9.5	5.8/5.8	–	●/●	●/●	NatB
	S22 A/B	14.6/14.6	9.9/9.9	–	O/–	O/O	–
	S23 A/B[d]	16.0/16.0	11.5/11.5	–	–	–	–
	S24 A/B[d]	15.3/15.3	10.5/10.5	●/–	●/–	●/●	NatA
	S25 A/B	12.0/12.0	10.3/11.1	–	–	O/–	–
	S26 A/B	13.5/13.4	10.8/11.6	–	–	O/–	–
	S27 A/B	8.9/8.9	9.4/9.5	–	O/O	O/–	–
	S28 A/B	7.6/7.6	10.8/11.4	–	●/●	●/–	NatB
	S29 A/B	6.7/6.7	11.1/10.8	–	O/O	–	–
	S30 A/B	7.1/7.1	12.2/12.2	–	O/O	–	–
	S31	17.2	10.7	–	–	–	–
Total	78			18	50	60	

●: N^{α}-Acetylated ribosomal protein. O: identified ribosomal protein.
[a] The calculated molecular weight and pI of ribosomal proteins were obtained from SWISS-PROT database.
[b] N^{α}-Acetylated ribosomal proteins were identified by 2-DE with an amino acid sequencer (Takakura et al.).
[c] N^{α}-Acetylated ribosomal proteins were identified by MALDI-TOF-MS (Arnold et al.).
[d] These ribosomal proteins A/B are used for duplicated genes that code proteins with identical sequence.

the following 17 ribosomal proteins in the *nat1* mutant were different in electrophoretic mobility from those in the normal strain (Fig. 1D); S2, S5, S7AB, S11, S14A, S15, S16, S17A, S18, S20, and S24 from the 40S subunit and L1, L4AB, L11B, L14A, L16AB, and L23 from the 60S subunit. These ribosomal proteins prepared from the *nat1* mutant had a shift toward the alkaline side of the gel that corresponds to the change in the protein isoelectric point expected from the lack of N^{α}-acetylation of an α-amino group. In addition, in a sample from the *nat3* mutant two ribosomal proteins, S21 and S28, had altered isoelectric points (Fig. 1E). However, no ribosomal proteins from the *mak3* mutant had changed isoelectric points (Fig. 1F). Although N^{α}-acetylation of ribosomal proteins was reported previously [12–14], this is the first time that ribosomal proteins L23 and S17 have been shown to be the substrates of NatA. The identified N^{α}-acetylated ribosomal proteins are listed in Table 1.

3.3. *Effects of the NAT deletion on cell growth*

It is well known that deletions or mutations of ribosomal protein genes influences both cell growth and temperature-sensitivity. We investigated the growth of the NAT mutants in the YPD medium at 30 °C (Fig. 2A). The doubling time was 1.4, 1.7, 4.0 and 1.4 h for the normal strain, *nat1*, *nat3*, and *mak3* mutants, respectively. The growth of the *nat1* and *nat3* mutants was decreased as compared to the normal strain, while the growth of the mak3 mutant remained unaltered, suggesting that the lack of protein N^{α}-acetylation by NatA and NatB affects cell growth. Next, we investigated the temperature sensitivity of the NAT mutants using 10-fold dilution spot assays performed on YPD plates at three different temperatures (20, 30, and 37 °C) (Fig. 2B). Growth of the normal and the NAT mutants was not significantly affected at 30 °C. In contrast, the *nat1* and *nat3* mutants showed slow growth phenotype at 37 °C.

3.4. *Effect of ribosomal protein N^{α}-acetylation on polyU-dependent poly-(Phe) synthesis*

The slower growth of the *nat1* and *nat3* mutants suggests that ribosomal protein N^{α}-acetylation may have an effect on protein synthesis, the most important function of ribosomes. Changes in the structure or function of yeast ribosomes are known to affect cell growth rate at a range of temperatures. In order to study the effect of ribosomal protein N^{α}-acetylation on protein synthesis, we performed polyU-dependent poly-(Phe) synthesis assays (Fig. 2C). The results demonstrated that the protein synthesis activities of 80S ribosomes purified from the *nat1* and *nat3* mutants were decreased by about 27% and 23%, respectively, as compared to the normal ribosomes. Thus, decreased protein synthesis activities in the *nat1* and the *nat3* mutants could be explained by the lack of N^{α}-acetylation of at least two or more ribosomal proteins from the list of 19 identified acetylated ribosomal protein (see above).

3.5. *Effect of the N^{α}-acetylation on polysome formation*

Polysome analysis in sucrose gradient is used to detect possible defects in ribosomal subunit assembly and proper organization of the ribosome chains that may cause protein synthesis alteration. As we observed decreased translation in the *nat1* and the *nat3* mutants it is possible that ribosome assembly or polysome organization is affected in the mutants. Therefore, we fractionated cell extracts from the normal and the NAT mutants in 7–47% sucrose density-gradient (Fig. 2D). Although the *nat1* and *mak3* mutants exhibited polysome profiles similar to the one from the normal strain, the *nat3* mutant clearly showed a defect in 80S ribosome assembly as the corresponding 80S ribosome peak was significantly decreased and 60S subunit peak was abnormally high. While no disruption of the polysome chains was observed, it appears that the altered ratio of 60S subunits to 80S ribosomes is either

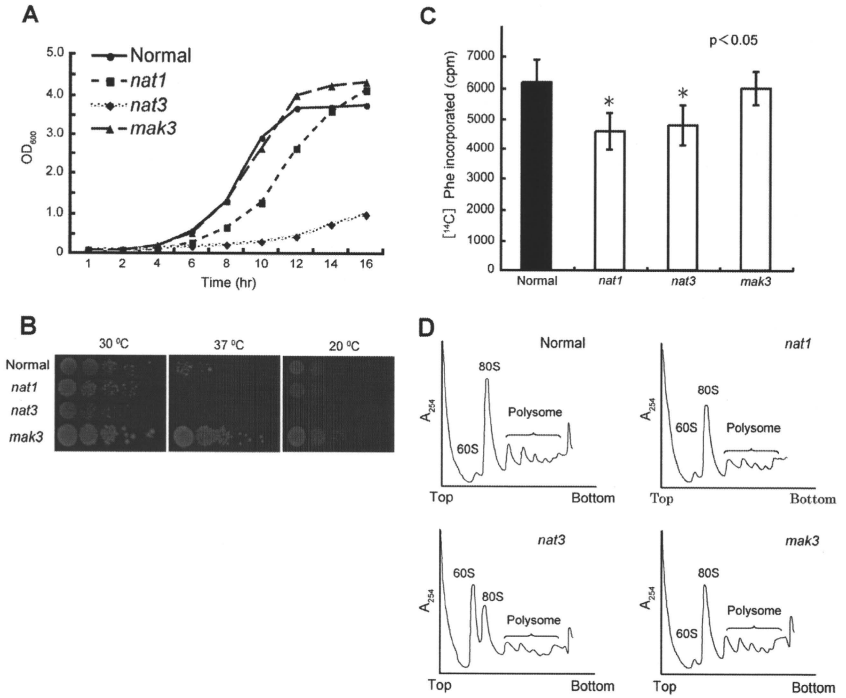

Fig. 2 – The effect of N^{α}-acetylation on cell growth and protein synthesis. (A) Growth curves of the normal strain and the NAT mutants. All strains were cultured in YPD at 30 °C until stationary phase. The absorbance of each culture was measured at 600 nm every 2 h. (B) Effect of three different temperatures (20, 30 and 37 °C) on the growth of the normal strain and the NAT mutants. Freshly grown yeast colonies were suspended in water, and 1/10 dilutions containing the same number of cells were spotted onto YPD plates. Spotted plates were incubated at 20, 30 and 37 °C for 3 to 4 days. (C) Effect of N^{α}-acetylation on polyU-dependent poly (Phe) synthesis. Purified 80S ribosomes from the normal strain and the NAT mutants were added to assay mixtures containing soluble factor S-100 from the normal strain and radioactive Phe residues, and incubated at 30 °C for 30 min. The radioactivity of the insoluble fraction, a measure of the incorporation of radioactive amino acids, was determined by liquid scintillation counter. The value shown in the figure was calculated by subtracting the value of the activity at 0 min. (D) The polysome profiles of the normal strain and the NAT mutants. Cytoplasmic extracts from the normal and the mutant strains were loaded onto 7–47% sucrose gradients, centrifuged, and fractionated. The fractions were collected from the top to the bottom with continuous A_{254} monitoring.

due to a failure to form 80S ribosomes or due to disruption in 40S subunit assembly. Thus, it is possible that decreased protein synthesis activity in the *nat3* mutant is at least in part due to a defect in ribosome assembly, whereas the altered activity in the *nat1* mutant is due to a difference of the fully assembled 80S ribosome.

3.6. *Sensitivity of the nat1 mutant to translation inhibitors*

In order to obtain more data on how NatA ribosomal protein N^{α}-acetylation affects ribosomal functions, we performed 1/10-dilution spot assays using YPD plates containing various antibiotics that bind to the ribosome and inhibit translation (Fig. 3A). We found that neither the normal strain nor the *nat1* mutant was sensitive to puromycin, which is known to cause premature chain termination during translation. However, both of the normal strain and the *nat1* mutant were sensitive to anisomycin and cycloheximide. Anisomycin is a competitive inhibitor of A-site binding that sterically hinders positioning of the acceptor end of A-site tRNA in the peptidyl transferase center (PTC) on the 60S subunit of the ribosome and cyclohexamide is known to interfere with the translocation step in protein synthesis by blocking translational elongation. These

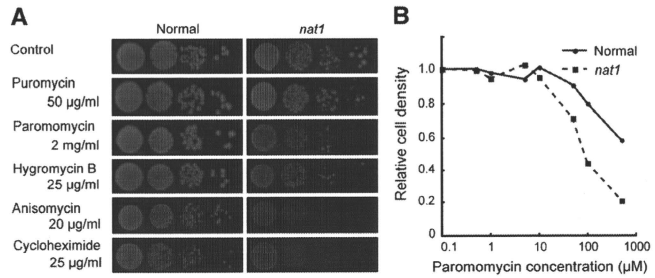

Fig. 3 – The effect of the NatA deletion on sensitivity to translation inhibitors. (A) The effect of various antibiotics on the growth of the normal strain and the *nat1* mutant. Freshly grown yeast colonies were suspended in water, and 1/10 dilutions starting at 0.1 OD_{600} were spotted onto YPD plates containing the indicated antibiotics. Spotted plates were incubated at 30 °C for 4 days. (B) The effect of paromomycin on growth of the normal strain and the *nat1* mutant. Freshly grown yeast colonies were cultured in YPD containing increasing concentrations of antibiotics until the culture without antibiotic reached an OD_{600} of 1–1.5, which was taken as 1.0.

results suggest that N^{α}-acetylation of ribosomal proteins by NatA has no specific effect on translocation or peptidyl transferase activity.

On the other hand, both paromomycin and hygromycin caused a specific decrease in the growth of the *nat1* mutant as compared to the normal strain. Therefore, we examined the effect of various paromomycin concentrations on growth of the *nat1* mutant (Fig. 3B) and found that sensitivity to paromomycin is increasing at higher antibiotic concentrations. Paromomycin is a translational error-inducing antibiotic that binds to the decoding center on the ribosome's 40S subunit and promotes conformational changes affecting formation of the codon–anticodon helix between mRNA and tRNA at the A-site. Thus, it appears that the N^{α}-acetylation of ribosomal proteins by NatA may be required to maintain a proper translational fidelity.

3.7. *The role of ribosomal protein N^{α}-acetylation in translational fidelity*

We investigated the *nat1* mutant's translational fidelity using a bicistronic reporter gene consisting of genes encoding a protein A peptide (14 kDa) and a FLAG peptide (1 kDa) (Fig. 4A). In this assay, if translation is accurate, the 14 kDa peptide is produced. If stop codon readthrough occurs, the 15 kDa peptide (which includes the FLAG tag) is produced. In the normal strain, we analyzed the affect of paromomycin on the level of a readthrough product in a concentration-dependent manner (Fig. 4B). We found that the readthrough product increased with increasing concentrations of paromomycin. Using this construct, we compared translational fidelity between the normal strain and the *nat1* mutant (Fig. 4C). The amount of a stop codon readthrough product in the *nat1* mutant was slightly higher than in the normal strain. Additionally, the level of the readthrough product in the *nat1* mutant was strongly influenced by the addition of paromomycin. Thus, N^{α}-acetylation by NatA is required for optimal translational termination. In addition, our reporter construct is useful for the analysis of translational fidelity in yeast.

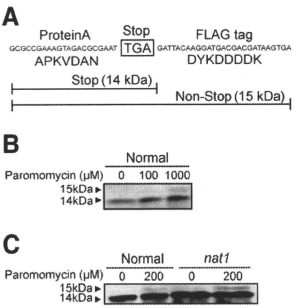

Fig. 4 – The role of ribosomal protein N^{α}-acetylation in translational readthrough activity. (A) The structure of the stop codon readthrough construct used in this study. The 14 kDa protein A fragment is a predominant translation product in the normal strain. The 14 kDa protein A fragment combined with the FLAG tag protein (1 kDa) which resulted in 15 kDa peptide is the mistranslated protein product. (B) Protein production in the normal strain with high concentration of paromomycin induced stop codon readthrough. Cells were grown in YPD containing the indicated concentration of paromomycin. Protein samples were loaded onto 15% SDS-PAGE and detected using Western blot with anti-peroxidase antibody. (C) Comparison of stop codon readthrough activity between the normal strain and the *nat1* mutant.